The Astrophysical Journal, 725:1688–1706, 2010 December 20 doi:10.1088/0004-637X/725/2/1688

GALAXY CLUSTERS IN THE *SWIFT*/BAT ERA. II. 10 MORE CLUSTERS DETECTED ABOVE 15 keV

M. Ajello[1], P. Rebusco[2], N. Cappelluti[3,4], O. Reimer[1,5], H. Böhringer[3], V. La Parola[6], and G. Cusumano[6]
[1] SLAC National Laboratory and Kavli Institute for Particle Astrophysics and Cosmology, 2575 Sand Hill Road, Menlo Park, CA 94025, USA; majello@slac.stanford.edu
[2] Kavli Institute for Astrophysics and Space Research, MIT, Cambridge, MA 02139, USA
[3] Max Planck Institut für Extraterrestrische Physik, P.O. Box 1603, 85740, Garching, Germany
[4] University of Maryland, Baltimore County, 1000 Hilltop Circle, Baltimore, MD 21250, USA
[5] Institut für Astro- und Teilchenphysik Leopold-Franzens-Universität Innsbruck Technikerstr. 25/8, 6020 Innsbruck, Austria
[6] INAF, Istituto di Astrofisica Spaziale e Fisica Cosmica di Palermo, via U. La Malfa 153, 90146 Palermo, Italy
Received 2010 April 26; accepted 2010 September 21; published 2010 December 1

ABSTRACT

We report on the discovery of 10 additional galaxy clusters detected in the ongoing *Swift*/Burst Alert Telescope (BAT) all-sky survey. Among the newly BAT-discovered clusters there are Bullet, A85, Norma, and PKS 0745-19. Norma is the only cluster, among those presented here, which is resolved by BAT. For all the clusters, we perform a detailed spectral analysis using *XMM-Newton* and *Swift*/BAT data to investigate the presence of a hard (non-thermal) X-ray excess. We find that in most cases the clusters' emission in the 0.3–200 keV band can be explained by a multi-temperature thermal model confirming our previous results. For two clusters (Bullet and A3667), we find evidence for the presence of a hard X-ray excess. In the case of the Bullet cluster, our analysis confirms the presence of a non-thermal, power-law-like, component with a 20–100 keV flux of 3.4×10^{-12} erg cm^{-2} s^{-1} as detected in previous studies. For A3667, the excess emission can be successfully modeled as a hot component ($kT \sim 13$ keV). We thus conclude that the hard X-ray emission from galaxy clusters (except the Bullet) has most likely a thermal origin.

Key words: acceleration of particles – galaxies: clusters: general – magnetic fields – radiation mechanisms: non-thermal – X-rays: general

Online-only material: color figures

1. INTRODUCTION

The study of clusters of galaxies at X-ray energies is key to understanding the mechanisms that heat the intracluster medium (ICM) and to measuring the pressure due to cosmic rays (CRs), magnetic fields, and turbulence. In particular, shock heating can be influenced by CRs if a significant part of the shock energy is transferred to charged particles. Indeed, large-scale shocks that form during the process of cluster formation are believed to be efficient particle accelerators (e.g., Sarazin 1999; Ryu & Kang 2003). Thus, the pressure support of CRs to the ICM might be relevant.

Not surprisingly, the role of CRs in the formation and evolution of clusters of galaxies has been much debated. Churazov et al. (2008) suggest that in massive galaxy clusters hydrostatic equilibrium is satisfied reasonably well, as long as the source has not experienced a recent major merger. On the other hand, other studies (e.g., Miralda-Escude & Babul 1995; Nagai et al. 2007) showed that the non-thermal pressure due to CRs, magnetic fields, and micro-turbulence can affect the mass estimates based on hydrostatic equilibrium. Knowing the importance of CRs, the mechanisms that heat the ICM and the frequency at which it is shocked, is crucial for the upcoming X-ray and Sunyaev–Zeldovich effect cluster surveys (see Ando & Nagai 2008).

The detections of extended synchrotron radio emissions (e.g., Willson 1970; Harris & Miley 1978; Giovannini et al. 1993; Giovannini & Feretti 2000; Kempner & Sarazin 2001; Thierbach et al. 2003) represent the main evidence that a population of non-thermal relativistic electrons exists in the ICM. These very same electrons can produce X-rays via inverse Compton (IC) scattering off cosmic microwave background (CMB) photons (e.g., Rephaeli 1979; Sarazin 1999), or via non-thermal bremsstrahlung (e.g., Sarazin 1999; Sarazin & Kempner 2000) or synchrotron radiation (Timokhin et al. 2004; Inoue et al. 2005). Detecting this non-thermal radiation is difficult because of the bright and dominant ICM thermal emission. Studying clusters above 15 keV, where the intensity of the thermal component decreases quickly, might prove to be an effective probe of the non-thermal emission processes. Indeed, in the past, the detection of non-thermal emission in the hard X-ray spectra of a few galaxy clusters has been reported (see, e.g., Kaastra et al. 2008 for a complete review). However, its actual presence and origin remain controversial (e.g., Rephaeli et al. 1987, 1999; Rephaeli & Gruber 2002; Rossetti & Molendi 2004; Sanders et al. 2005; Renaud et al. 2006; Fusco-Femiano et al. 2007; Lutovinov et al. 2008; Molendi & Gastaldello 2009).

In a first paper (Ajello et al. 2009a), we reported about the detailed analysis of 10 galaxy clusters serendipitously detected in the *Swift*/Burst Alert Telescope (BAT) all-sky survey above 15 keV. In that study, we concluded that there was no significant evidence for the existence of hard X-ray excesses detected in the spectra of clusters above the BAT sensitivity. In this paper, we report the analysis of 10 additional clusters that have been recently detected, thanks to the deeper exposure, in the ongoing BAT survey. We combine BAT and *XMM-Newton* data to find the best spectral fit. Assuming that there is a non-thermal emission due to IC scattering on CMB photons, we estimate the upper limit of its flux in the 50–100 keV band. This information allows us to estimate the intensity of the magnetic fields in these galaxy clusters.

Throughout this paper, we adopt a Hubble constant of $H_0 = 70$ km s^{-1} Mpc^{-1}, $\Omega_M = 0.3$, and $\Omega_\Lambda = 0.7$. Unless otherwise stated errors are quoted at the 90% confidence level (CL) for one interesting parameter and solar abundances are determined using the meteoritic values provided in Anders & Grevesse (1989).

2. CLUSTERS IN THE *SWIFT*/BAT SURVEY

BAT (Barthelmy et al. 2005), on board the *Swift* satellite (Gehrels et al. 2004), represents a major improvement in sensitivity for imaging of the hard X-ray sky. BAT is a coded mask telescope with a wide field of view (FOV; $120^\circ \times 90^\circ$ partially coded) sensitive in the 15–200 keV domain. As shown in several works (e.g., Ajello et al. 2008a, 2009b; Tueller et al. 2010), thanks to the deep exposure, BAT reaches sub-mCrab (e.g., $< 10^{-11}$ erg cm^{-2} s^{-1}) sensitivities in the entire high-latitude sky. This already allowed BAT to detect 10 galaxy clusters above 15 keV after ∼2 years of all-sky exposure (see Ajello et al. 2009a, for details). With ∼6 years of all-sky exposure acquired, the sensitivity of BAT has increased substantially leading to the detection of almost 1000 sources in the hard X-ray sky (see Cusumano et al. 2010 for details). Here, we present a detailed spectral analysis of 10 galaxy clusters detected in the BAT survey of Cusumano et al. (2010).

2.1. Analysis of Swift/BAT Data

BAT makes images of the sky thanks to a coded mask (with a random pattern) placed above a position sensitive detector plane (see Barthelmy et al. 2005 for details). The sky radiation passing through the aperture is coded by the mask pattern and recorded in the detector plane. The pattern of the mask is such that a source at a given position in the FOV casts a unique shadow onto the detector plane and thus its emission can be easily deconvolved. The randomness of the mask pattern ensures that the cross-talk between sources (e.g., some flux from a given source is wrongly attributed to another one) at different positions in the FOV is minimum. Moreover, to minimize this and other systematic uncertainties that can arise in the BAT survey, *Swift* adopts a random roll-angle strategy when pointing at the same position in the sky. This means that whenever *Swift* is pointing at a given direction in the sky, the roll angle (e.g., the angle on the plane orthogonal to the pointing direction) is chosen randomly within a range of the nominal (e.g., within $\pm 2^\circ$) pointing. This ensures that pointings are never exactly the same and that sources never fall in the same relative positions in the BAT FOV.

A decoding procedure is required in order to reconstruct the original sky image. A variety of methods can be used to reconstruct the sky image in the case of a coded mask aperture (see Skinner et al. 1987; Ajello et al. 2008a, for a general discussion on reconstruction methods). Among them, standard cross-correlation of the shadowgram (e.g., the information recorded on the detector plane) with a deconvolution array, the mask pattern, via fast Fourier transforms (FFTs), is the most often used. Generally, sky images are obtained for each individual observation, where an observation is defined as a period during which the attitude is stable and constant. Subsequently, another procedure, such as resampling and reprojecting, is needed in order to assemble the final all-sky image. As discussed in the appendix in Ajello et al. (2008c), the *balanced correlation* (Fenimore & Cannon 1978) used to deconvolve BAT observations and source spectra performs a standard background subtraction (see the above references for the exact implementation of this method). However, this technique works well as long as the background in the array is flat and not correlated with the mask pattern. The background in the BAT array is not flat due to the presence of many background components, the brightest of which is (below ∼60 keV) the cosmic X-ray background (see Ajello et al. 2008b for details). Thus, the balanced correlation alone provides imperfect results and produces a noticeable background contamination in the sky observations and in the source spectra. This background contamination has been estimated (see Ajello et al. 2008c) to be $\leqslant 2\%$ of the Crab Nebula intensity in the 14–195 keV band (e.g., the BAT band). Thus, this contamination does not pose problems for strong sources, but becomes very relevant for the (spectral) analysis of faint objects with ∼mCrab intensities as the clusters of this work. In order to correct for this residual background contamination, we use the recipe presented in Ajello et al. (2008c). We use several templates[7] of the BAT background (for each channel) which are fit together with the contribution of point sources to the BAT detector counts. In each observation, the residuals are analyzed to check for additional structures and deviation from Gaussian statistics. If those are found, then thousands of residual maps are averaged together (in image coordinates) to create a *blank field* observation.[8] These *blank field* observations become part of our template library of background models and are fit once again to any observations that are being used. The process of residual inspection and template creation is repeated until the residuals do not show any systematic feature. For a given observation, the last template model to be added is generated from observations which are close to it in time. This ensures that long-term variation in the BAT background (due, e.g., to the orbit, activation of the spacecraft, noisy pixels, etc.) is correctly taken into account.

Adopting this technique and filtering the data in the way described in detail in Ajello et al. (2008a), we extracted a 15–195 keV spectrum for the 10 galaxy clusters of this analysis. We used all the available observations at the time of this work (approximatively from 2005 to 2010 March) resulting in an average exposure larger than 14 Ms at each of the 10 positions. It has already been shown that spectra extracted with this method are reliable and accurate over the entire energy range (see Section 2.3 of Ajello et al. 2009a for details).

2.2. Studying "Extended" Sources with Swift/BAT

Coded mask telescopes are designed and optimized for the study of point-like sources (e.g., see Ajello et al. 2008b and references therein). Formally the mask acts as a filter, canceling out those signals (celestial and not) whose spatial frequency is larger than the spatial frequencies of the mask tiles. This means that if an X-ray source extends over an area which is larger than the projection of the mask tile on the sky (i.e., 22.′4 or, which is the same, the full width at half-maximum, FWHM, of the BAT point-spread function, PSF) then part of the X-ray flux is *necessarily lost* in the background. In simpler words, if a source is extended, then its shadow (produced when the radiation passes through the mask) on the detector plane looses part of its contrast (i.e., the mask is illuminated from all sides). The limiting case is represented by the cosmic X-ray background, which extending over the entire sky, is completely removed by the BAT mask. Indeed in order to measure the cosmic background, different non-standard techniques have to be used (Ajello et al. 2008b).

Clusters of galaxies are X-ray sources extending up to $\sim 1^\circ$. In our first work, Ajello et al. (2009a), we showed that all the clusters detected by BAT are consistent with being point-like sources (for BAT) with the exception of Coma which is clearly resolved. Given the properties of coded masks expressed above, it is a good thing that clusters are seen as point-like sources. Indeed, in this case the flux measurement is correct while it is not if the source is *detected* as extended.

[7] For reference, see the description of the *batclean* tool available at http://heasarc.nasa.gov/lheasoft/ftools/headas/batclean.html.

[8] Working in detector coordinates ensures that the contribution of any unsubtracted point source is averaged out.

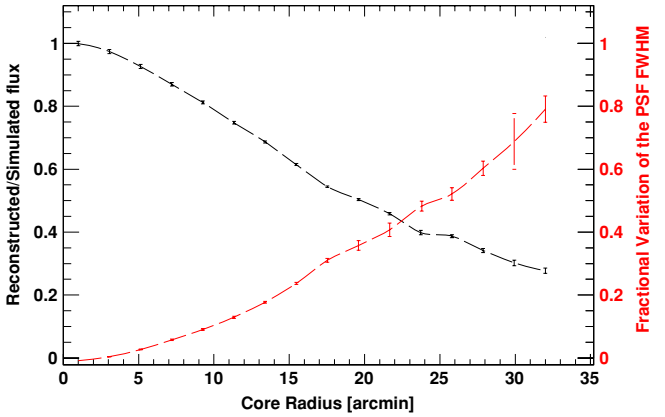

Figure 1. Suppression of the source flux (solid line) due to the source extension as a function of core radius (r_c) for an emission profile that follows a beta model (see Section 2.2 for details). Error bars are of statistical origin and reflect the uncertainty in the reconstructed quantities. The dashed line shows the fractional increase of the FWHM of the source PSF (with respect to the PSF for a point-like source) when the source is "resolved" by BAT. For a cluster with a core radius of 30′, the FWHM is ∼80% larger than the point-like source FWHM.

(A color version of this figure is available in the online journal.)

In order to quantify this effect in more detail, we performed several Monte Carlo simulations. We simulated an extended source whose surface brightness profile can be approximated by a *beta model* of the form

$$F(r) \propto \left[1 + \left(\frac{r}{r_c}\right)^2\right]^{0.5-3\beta}, \quad (1)$$

where r_c is the core radius and β is typically in the 0.5–0.8 range (see, e.g., Ettori et al. 1998; Ajello et al. 2009a). We then reconstructed the sky image and detected the simulated source measuring its flux and the PSF FWHM. Simulations were performed, in the 15–55 keV band,[9] for several core radii and for a fixed β of 0.6. The results of this exercise are reported in Figure 1. It is clear that a substantial part of the source flux is lost if clusters have a core radius larger than 5′. This effect is a function of the emissivity profile of the source and depends on it. If we were considering a source with a Gaussian emission profile or a uniform profile (e.g., a disk-like emission) then the flux suppression would be even stronger. The presence of a cool core acts in the opposite direction, indeed in this case a large part of the cluster's emission is confined within the inner few arcminutes from the core (normally within the core radius) where the flux suppression (due to source extension) is negligible. Moreover, Figure 1 gives a powerful tool to understand when the flux suppression takes place. Indeed, in all these cases the FWHM of the source is larger than the pointas it is apparent from this figure,-like one (i.e., 22.′4). Coma which is resolved by BAT can be used as an example. Indeed, adopting a core radius of $r_c = 10.'7$ (see, e.g., Lutovinov et al. 2008), we can estimate from Figure 1 that the measured FWHM should be ∼26′. This is found to be in good agreement with the results reported in Ajello et al. (2009a). Moreover, from the same graph we can estimate that the flux suppression is ∼25%. The next most extended clusters reported in Ajello et al. (2009a) are Ophiucus and Perseus. Ophiucus with a core radius of 3.′2 (Watanabe et al. 2001) is not resolved by BAT and thus the flux suppression is negligible. Perseus has a core radius of 4.′7 (Ettori et al. 1998) and thus at the limit where the flux suppression might start playing a role. However, Perseus has a bright cool core whose emission profile can be modeled with a power law (e.g., see Ettori et al. 1998, and references therein). This concentrates most of the cluster's emission in the core which is never resolved by BAT. Hence, Perseus is detected as a point-like object. The majority of the clusters detected by BAT, either those reported here or those described in Ajello et al. (2009a), are detected as point-like objects. Norma (reported in this work) with a core radius of ∼10′ like Coma, is also resolved by BAT. However, its marked northwest elongation and the presence of a bright nearby active galactic nucleus (AGN) make its case more complex that the simple spherically symmetric case discussed here. This will be discussed in detail in Section 3.8.

To summarize this section, we note that coded mask telescopes are optimized for the study of point-like objects and can be used for the study of (intrinsically) extended objects only if these are detected as point-like (e.g., for a beta model this is true if the core radius is less than 5′). If an object is detected as extended, then part of its flux (depending on the source brightness profile) is suppressed. The deviation of the PSF from the point-like PSF can be used to understand whether this effect is present. Among all the clusters detected by BAT, Coma and Norma (see next sections) are the only two sources which are *extended* in BAT and part of the source flux is lost in the BAT background. All the other clusters detected by BAT are not resolved by BAT and BAT can be safely used for the study of their emission.

2.3. Analysis of XMM-Newton Data

For all the clusters, we extracted a 0.5–8.0 keV spectrum using publicly available *XMM-Newton* (EPIC-PN) observations. The details of these observations are reported in Table 1.

For each observation, *XMM-Newton* data are screened, filtering for periods of flaring background. This is done by examining the light curve in the 10–12 keV band and determining the rate of the quiescent background (the rate outside of the flaring episodes). For all the observations reported in this analysis, this was very close to 0.5 counts s^{-1} in agreement with, e.g., Nevalainen et al. (2005 and references therein). However, this is not sufficient for filtering out flaring episodes that produce a soft background component (e.g., Nevalainen et al. 2005; Carter & Read 2007). We thus inspect the light curve in the 1–5 keV band extracted in an annulus of inner radius 10′ and outer radius 12′. We filter out all those time bins that deviate more than 3σ from the average quiescent background (determined through a Gaussian fit to the histograms of the rates).

We extracted the cluster spectrum using a single extraction region with a radius of ∼10′. This is partly motivated by (1) the extent of the *XMM-Newton* EPIC-PN CCD (∼12′ in radius), (2) the fact that we use the two outer arcminutes to perform background filtering, and (3) the fact that for a typical beta profile (e.g., core radius of 3.′8 and $\beta = 0.7$) this selection includes up to 94% of the entire cluster emission and more than that if the cluster has a cool core. The fact that the BAT PSF is consistent with the point-like one for all the clusters in this analysis (except Norma) suggests that the hard X-ray emission (above 15 keV) is coming from the inner part of the cluster. If this were not the case, we would have observed a significant deviation in the FWHM of the BAT PSF. Table 1 shows the dimension in physical units (e.g., kpc) of the extraction radius of 10′ at the redshift of the source.

[9] The results of this analysis do not change if a different band is chosen.

Table 1
XMM-Newton Observations of BAT Clusters of Galaxies

Name	R.A.[a] (J2000)	Decl.[a] (J2000)	Date	OBSID	Exposure[b] (ks)	Radius[c] (kpc)
A85	10.4303	−9.3483	2002-01-07	0065140101	10.0	635.4
A401	44.7395	13.5837	2002-02-04	0112260301	13.6	823.8
Bullet	104.6176	−55.8974	2000-10-21	0112980201	46.7	2460.0
PKS 0745-19	116.8758	−19.3462	2000-10-31	0105870101	28.3	1100.0
A1795	207.1856	26.5928	2000-06-26	0097820101	66.5	702.6
A1914	216.5013	37.8071	2002-12-18	0112230201	25.8	1663.8
A2256	256.0720	78.6301	2006-08-04	0401610101	50.4	662.4
A3627	243.6066	−60.8348	2004-09-19	0204250101	22.6	204.1
A3667	302.9667	−56.8407	2004-05-03	0206850101	67.3	636.1
A2390	328.4471	17.7516	2001-06-19	0111270101	23.1	2079.6

Notes.
[a] *Swift*/BAT coordinates are from the work of Cusumano et al. (2010).
[b] Nominal *XMM-Newton* exposure before data screening.
[c] Extraction radius in physical units corresponding to the region of radius 10′ around the BAT position used to extract the *XMM-Newton* spectrum of the cluster.

The level of the background was evaluated using blank-sky observations[10] (e.g., see Lumb et al. 2002; Read & Ponman 2003; Nevalainen et al. 2005) which are described in detail in Carter & Read (2007). The black fields were selected from the same sky region as the observation under analysis and with a similar foreground absorbing column density. These fields were then reprojected to the source (sky) coordinates system and processed in a similar way as the observation under analysis. For each cluster, a background spectrum has been extracted from the exact same 10′ region as the cluster. To allow for different intensities of the background components (between the source and the "background" observations), we renormalized the background spectrum by the ratio of the total emission in the 10–12 keV band in the annulus with inner and outer radii of 10′ and 12′, respectively (see also Molendi & Gastaldello 2009).

The results of the background subtraction change slightly by varying this renormalization constant within its error, as well as changing the extraction annulus of the background or the thresholds for the removal of the flaring episodes (in the hard and the soft bands). We noticed that the spectral results are robust for variation of the aforementioned parameters if a systematic uncertainty of ∼2% is applied to our background subtracted spectra. We thus employed this systematic uncertainty connected to the background subtraction, in the 0.5–8 keV band, when fitting the *XMM-Newton* data. Finally, all the spectra were rebinned in order to have a minimum of 50 counts ($\geqslant 7\sigma$) per bin.

The most distant clusters in our sample provide a test bed for checking the goodness of the background subtraction employed in this work. Indeed, for the Bullet cluster, PKS 0745-19 and A2390 is possible to find spatial regions of the EPIC-PN CCD that are the least contaminated by the cluster emission. These regions provide a clean way to determine the background spectrum which suffers from different systematic uncertainties[11] with respect to the use of blank fields. In all these cases, we found that within the aforementioned systematic uncertainty, the two background subtracted spectra (e.g., the one that uses blank field observations and the one that uses part of the CCD which is not contaminated by the cluster emission) are in good agreement. One such example is reported in Figure 2, which shows the two background subtracted spectra (generated with the two different techniques described above) of PKS 0745-19 fitted with a single-temperature thermal model. As is apparent from this figure, there is very good agreement between the two spectra.

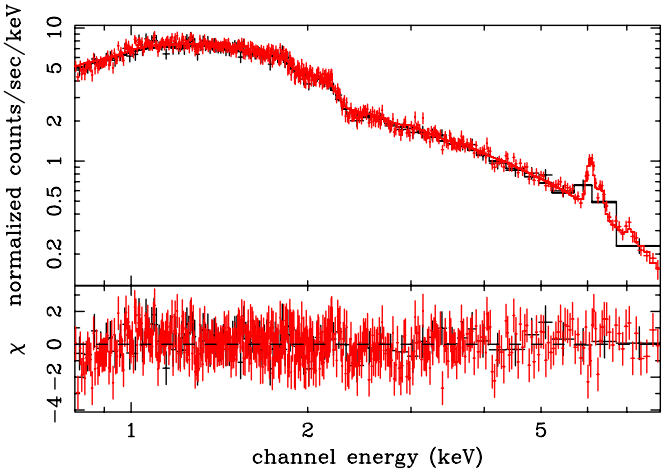

Figure 2. Spectra of PKS 0745-19 using two different background subtraction techniques: blank field observations (in red) and an extraction region free of the cluster's emission (in black). The spectra were rebinned differently to simplify the comparison.

(A color version of this figure is available in the online journal.)

2.4. Point-like Sources in the XMM-Newton Fields

Given the extent of its PSF, BAT is unable to discriminate the cluster's emission from that of nearby point sources which fall in the cluster's region. Thus, if present these sources would contaminate with their signals the cluster's emission as seen by BAT. For this reason, when analyzing *XMM-Newton* data jointly with BAT, we do not filter out the point sources which are clearly resolved and detected by *XMM-Newton*. However, we employ two different approaches to determine whether these sources contaminate in any way the total X-ray signal in the BAT band.

In the more general approach, we evaluate the contamination from point sources using the 2XMM catalog (Watson et al. 2009)

[10] Blank observations are described and made available at http://xmm.vilspa.esa.es/external/xmm_sw_cal/background/blank_sky.shtml#BGfiles.
[11] The main systematic uncertainty is that the background spectrum is extracted from a region different from the region used to extract the cluster's spectrum.

Table 2
Summed X-ray Emission from All the Point-sources Detected by *XMM-Newton* in the Fields of the Clusters

Name	Count Rate[a] (count s^{-1})	No. Sources	$Flux_{0.2-12\,keV}$ (erg cm^{-2} s^{-1})	$Flux_{15-55\,keV}$ (erg cm^{-2} s^{-1})
A85	0.23	10	5.61×10^{-13}	1.78×10^{-13}
A401	0.10	4	3.72×10^{-13}	1.18×10^{-13}
Bullet	0.10	4	2.38×10^{-14}	7.55×10^{-14}
PKS 0745-19	0.63	14	4.88×10^{-12}	1.55×10^{-12}
A1795	1.76	13	4.28×10^{-12}	1.36×10^{-12}
A1914	0.34	19	8.07×10^{-13}	2.56×10^{-13}
A2256	0.21	10	4.98×10^{-13}	1.58×10^{-13}
A3627	0.15	1	3.56×10^{-13}	1.13×10^{-13}
A3667	0.37	27	6.90×10^{-13}	2.19×10^{-13}
A2390	0.51	16	12.1×10^{-13}	3.85×10^{-13}

Note. [a] Summed count rate of all sources detected by *XMM-Newton* in the 0.2–12 keV band.

which contains all point sources detected in the *XMM-Newton* fields including the observations used in this work (e.g., 1). From the 2XMM catalog, we select all the point sources detected in the 0.2–12 keV band, with a likelihood probability of being spurious $-\ln(P) > 15$ and within 10′ from the *Swift*-BAT centroid. The count rate of all the sources in the FOV has been summed and converted by extrapolation into 15–55 keV fluxes in units of erg cm^{-2} s^{-1}. In this conversion, we assumed that the spectra of these sources were represented by a power law with a photon index of $\Gamma = 2$, absorbed by a cold material with column-density $N_{\rm H}$ equal to the Galactic value. We believe that this approach will yield conservative estimates for the contamination to the 15–55 keV signal produced by point-like sources. Indeed, by assuming a power-law spectrum we implicitly assumed that all sources detected by *XMM-Newton* are AGNs, while it is known that a large fraction of the sources detected in clusters' region show a thermal spectrum (see Figure 10 in Finoguenov et al. 2004 and references therein) and thus will have a negligible >10 keV emission. As shown in Burlon et al. (2010), the average broadband 1–200 keV *intrinsic*[12] spectra of AGN are compatible with a power law with a photon index of $\sim$2.0. Our estimates are reported in Table 2. For most of the clusters in this analysis, the estimated contamination from point sources is a factor $\sim$50 below the total (cluster plus sources) emission measured by BAT (see Table 3 for details), and thus negligible. For only three clusters, PKS 0745-19, A1795, and A2390, the contamination might be relevant (still a factor $\sim$5 below the total flux).

In the second approach, we study the *XMM-Newton* observations closely and extract the spectrum of the brightest sources (up to five) in the field. The characterization of their spectra in the 0.5–8.0 keV band allows us to make a solid prediction (i.e., without assumptions) of the contaminating signal in the BAT band. The findings will be discussed case by case in the next sections.

2.5. Joint Analysis of XMM-Newton and Swift/BAT Data

Spectral analysis of *XMM-Newton* and *Swift*/BAT data has been performed, for all the clusters, using XSPEC (version 12.5.1 in Arnaud 1996). Observations of the Crab Nebula showed that, in principle, the inter-calibration of the two instruments is good within $\sim$5%. Indeed, as reported in Kirsch et al. (2005), the Crab Nebula 0.3–10 keV spectrum as observed with the EPIC-PN can be modeled as an absorbed power law with a photon index of 2.125, a normalization of 8.86, and an absorbing column density of 4.08×10^{21} atoms cm^{-2}. For BAT,[13] the Crab Nebula 15–200 keV spectrum is compatible with a power law with a photon index of 2.15 and normalization of 10.17. Thus, for the 15–55 keV band (where most of the clusters' signal is concentrated for BAT) the two Crab Nebula parameterizations yield a flux of 1.21×10^{-8} erg cm^{-2} s^{-1} and 1.28×10^{-8} erg cm^{-2} s^{-1} for *XMM-Newton* and BAT, respectively. Thus, we expect the inter-calibration of the two instruments to be close to unity (within $\sim$5%). However, one must take into account that the Crab Nebula is a very bright target for *XMM-Newton* and in order to avoid pile-up problems the observations presented in Kirsch et al. (2005) were performed in "Burst Mode" (see Kirsch et al. 2005 for details) rather than the Full-Frame Mode normally used for studying diffuse sources with *XMM-Newton*. Thus, the same inter-calibration between *XMM-Newton* and BAT might not necessarily apply in this case. However, Burlon et al. (2010) performed spectral fitting of 12 faint AGNs using *XMM-Newton* (with the EPIC-PN in Full-Frame Mode) and *Swift*/BAT. In all these cases, the inter-calibration between the two instruments has been found to be compatible with unity. As a strategy in the spectral fitting presented in the next section, we employed a normalization constant to take into account differences in the calibrations of the *XMM-Newton* and BAT instruments. This constant has been fixed to 0.95 to take into account the different Crab Nebula spectra as observed with the two instruments. However, we performed some tests with the joint data sets of this paper and found out that changing the inter-calibration constant by $\pm$10% produces a negligible change (e.g., less than 1%) in the best-fit temperatures and their uncertainties. Thus, the results that will be presented are robust against variation of the aforementioned inter-calibration constant. The reason for the small variation of the temperature with the inter-calibration constant lies in the different signal-to-noise ratios of the two data sets. Indeed, in a joint fit the best-fit temperature is entirely constrained by the signal in the *XMM-Newton* band and a small variation of the inter-calibration constant (e.g., moving the less significant BAT data up or down around the best fit) does not change the results. We also checked that leaving this constant free to vary did not produce any appreciable improvement in the fit (in terms of goodness of fit) for all the clusters presented in this work.

We started fitting all the spectra with a single-temperature thermal model (APEC) with absorption fixed at the Galactic value. Only if the value of the χ^2/dof was significantly greater than 1, we tried to add a second thermal model or a power law. In this case, we chose the model which produced the best improvement in the fit (evaluated using the *F*-test) and the best residuals. In all spectral fits, all the parameters are tied together within the two data sets (e.g., *XMM-Newton* and BAT).

In order to test which is the maximum level of non-thermal emission which is allowed by our data, a power law has been added to the best-fit model of every cluster. The power-law index has been fixed to 2.0, which is a value generally accepted for the non-thermal hard X-ray component generated by IC of relativistic electrons off CMB photons (e.g., Reimer et al. 2004; Nevalainen et al. 2004). We then let the power-law

[12] Photoelectric absorption caused by the circumnuclear material around the source will make the AGN spectra look harder in the <10 keV band, but the >10 keV continuum will be mostly unaffected (see Burlon et al. 2010 for details).

[13] See http://swift.gsfc.nasa.gov/docs/swift/analysis/bat_digest.html for details.

Table 3
Spectral Properties of BAT-detected Galaxy Clusters (Errors are 90% CL)

Name	z	Flux[a] (10^{-12} cgs)	L_x[a] (10^{43} erg s^{-1})	kT (keV)	Γ/kT	Model	χ^2/dof
A85	0.0521	$5.15^{+0.81}_{-0.83}$	$3.81^{+0.52}_{-0.82}$	$6.09^{+0.43}_{-0.29}$	$1.72^{+0.32}_{-0.06}$	apec + apec	602.1/619
A401	0.074	$6.39^{+0.91}_{-0.84}$	$9.98^{+1.48}_{-1.47}$	$8.61^{+0.60}_{-0.46}$	$2.05^{+0.65}_{-0.45}$	apec + apec	732.4/652
Bullet	0.296	$5.10^{+2.68}_{-1.50}$	176^{+65}_{-45}	$14.77^{+1.13}_{-0.72}$	$1.86^{+1.25}_{-0.14}$	apec + pow	501.7/511
PKS 0745-19	0.103	$6.93^{+0.89}_{-1.16}$	$23.2^{+2.9}_{-3.4}$	$7.96^{+0.68}_{-0.54}$	$2.16^{+1.08}_{-0.56}$	apec + apec	587.1/578
A1795	0.062	$2.05^{+0.18}_{-0.18}$	$2.37^{+0.23}_{-0.20}$	$4.82^{+0.10}_{-0.11}$	...	apec	892.1/1275
A1914	0.171	$4.29^{+1.09}_{-1.04}$	$46.6^{+9.9}_{-9.5}$	$11.14^{+1.13}_{-1.09}$	...	apec	355.1/351
A2256	0.0581	$4.46^{+1.15}_{-1.22}$	$4.04^{+1.10}_{-1.07}$	$8.84^{+0.66}_{-0.61}$	...	apec	445.6/445
A3627[b]	0.0168	$8.00^{+1.32}_{-5.81}$	$0.48^{+0.08}_{-0.75}$	$11.6^{+6.2}_{-3.3}$	...	brem	14.7/14
A3667	0.0556	$7.30^{+1.44}_{-1.84}$	$5.65^{+1.07}_{-1.12}$	$4.00^{+0.49}_{-0.53}$	$13.5^{+6.9}_{-2.2}$	apec + apec	569.8/542
A2390	0.231	$2.13^{+0.26}_{-0.25}$	$52.5^{+5.5}_{-4.7}$	$13.08^{+4.15}_{-2.69}$	$3.76^{+2.80}_{-1.61}$	apec + apec	394.5/372

Notes.
[a] Flux and luminosities are computed in the 15–55 keV band.
[b] For this cluster only BAT data were used.

normalization vary until the $\Delta\chi^2$ increment was larger than 2.7(6.64). According to Avni (1976), this gives the 90% (99%) CL on the parameter of interest. This allows us to investigate the level of non-thermal flux which is consistent with our data. In the next sections, the details of the spectral analysis of each single cluster are reported.

3. SPECTRAL ANALYSIS OF INDIVIDUAL CLUSTERS OF GALAXIES

3.1. A0085

A85, a galaxy cluster at $z = 0.0521$, has been detected for the first time in the X-ray band by Ariel V, thus it is one of the first galaxy clusters ever detected in X-rays (Mitchell et al. 1979; McHardy 1978). A detailed analysis performed with *Einstein* (Jones & Forman 1999) showed that the ICM temperature is in the 7–9 keV range. *ROSAT* observations (Prestwich et al. 1995) revealed that the temperature and surface brightness structures of A85 are not regular, implying that the cluster is dynamically disturbed. At the same time, the high central gas density indicates the presence of a cool core. Ensslin et al. (1998) showed that A85 has recently experienced a major merging, as indicated by the presence of a radio relic. The estimate of the magnetic field intensity is, for the radio relic, of the order of $B \sim 2.6\,\mu$G (Ensslin et al. 1998). Slee et al. (2001), using high-resolution radio observation, determined that the flux and spectral index of the relic at 1.425 GHz are $S_R = 40.9$ mJy and $\alpha = 3$.

The combined *XMM-Newton* and *Swift*/BAT data set when fit by a single thermal model produces a χ^2/dof = 738.8/622, leaving unsatisfactory residuals at high energy. We thus added an additional thermal model to the fit which produces a significant improvement in the fit ($\Delta\chi^2 \approx 140$ for three additional parameters). The best fit (χ^2/dof = 602.1/619) temperatures are $6.09^{+0.43}_{-0.29}$ keV and $1.72^{+0.32}_{-0.06}$ keV, while the respective metallicities are $0.33^{+0.04}_{-0.03}$ and $0.15^{+0.04}_{-0.03}$. The low-temperature component accounts for the cool core of the cluster. Our results are in good agreement with the one reported by Durret et al. (2005) using *XMM-Newton* data alone.

We also tried to add a power-law model to the single thermal model. The fit improves with respect to the single-temperature thermal model with a $\Delta\chi^2 = 59$ for two additional degrees of freedom. The best-fit temperature in this case becomes $5.09^{+0.14}_{-0.16}$ keV and the photon index of the power law $2.68^{+0.19}_{-0.13}$. However, the $\Delta\chi^2$ is noticeably larger when the sum of two thermal models is fit to the data and we consider this model to be the best representation of our data set (parameters reported in Table 3). Both spectral fits are reported in Figure 3.

We derive a 99% upper limit on any non-thermal component of 2.51×10^{-12} erg cm^{-2} s^{-1} in the 50–100 keV band. The upper limit on the non-thermal luminosity in the 20–80 keV band is 3.62×10^{43} erg s^{-1}. When converted to the cosmology used by Nevalainen et al. (2004; $H_0 = 50$ km s^{-1} Mpc^{-1}, $q_0 = 0.5$, and $\Lambda = 0$) this becomes 6.68×10^{43} erg s^{-1} which is in agreement with the value of $10.7^{+6.3}_{-6.3} \times 10^{43}$ erg s^{-1} reported in Nevalainen et al. (2004).

3.2. A401

A401, at $z = 0.074$, is part of a cluster pair with A399 which is in a pre-merging state (e.g., Karachentsev & Kopylov 1980; Fujita et al. 1996, and references therein). It is a rich cluster with a temperature of the ICM in the 7–8 keV range (Fujita et al. 1996). Recently, using *XMM-Newton*, Sakelliou & Ponman (2004) found an average ICM temperature of $7.23^{+0.17}_{-0.21}$ keV. A401 was one of the first clusters, along with Coma, that were discovered to host an extended radio emission (Harris & Romanishin 1974). This radio halo was recently confirmed by deep Very Large Array (VLA) observations (Bacchi et al. 2003). The intensity at 1.4 GHz was found to be $S_R = 17 \pm 1$ mJy.

The BAT spectrum is fit well by a bremsstrahlung model with a plasma temperature of $7.79^{+5.30}_{-2.86}$ keV. The combined *XMM-Newton*-BAT data set is reasonably well fit (χ^2/dof = 766.3/655) by a single thermal model with a temperature of 7.19 ± 0.17 keV and an abundance of 0.25 ± 0.03 solar. Still, adding a second thermal model improves the fit substantially ($\Delta\chi^2 = 33.9$ for three additional parameters). The temperature and abundance of the hot component are, respectively, $8.61^{+0.60}_{-0.46}$ keV and $0.30^{+0.04}_{-0.04}$. Those of the cold component are, respectively, $2.05^{+0.65}_{-0.45}$ keV and $0.16^{+0.11}_{-0.08}$. This fit is shown in the left panel of Figure 4.

We also tried a fit with the sum of a thermal model and a power law (see the right panel of Figure 4). The best-fit temperature and power-law photon index are, respectively, $7.55^{+0.26}_{-0.27}$ keV and $2.16^{+0.63}_{-0.26}$. The improvement in the goodness of fit, with respect to the single thermal model, is $\Delta\chi^2 = 9.1$ for two

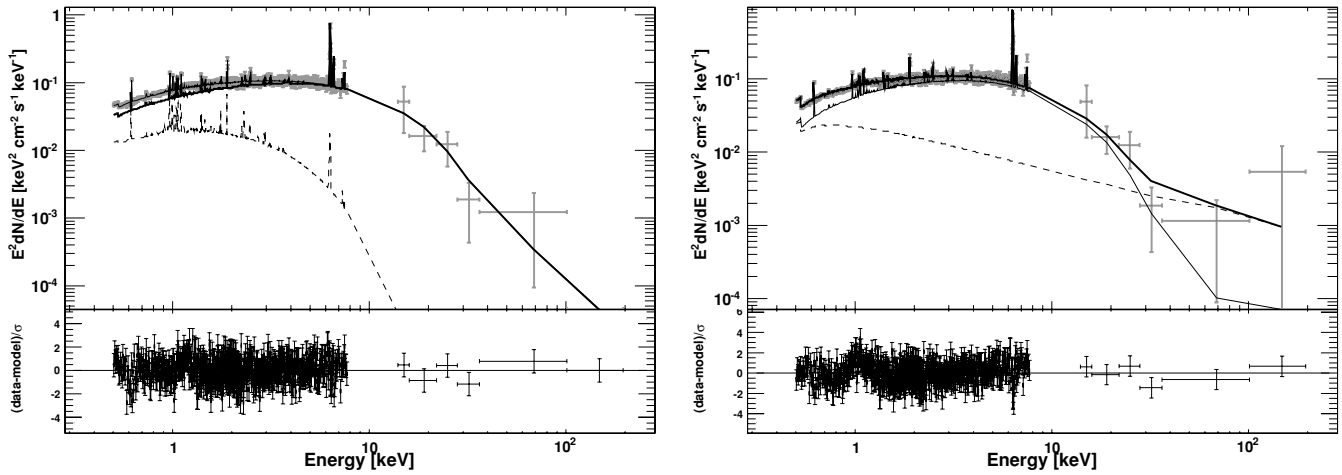

Figure 3. Left panel: spectrum of A85 fitted with the sum of two thermal models. Right panel: spectrum of A85 fitted with the sum of a thermal model and a power law.

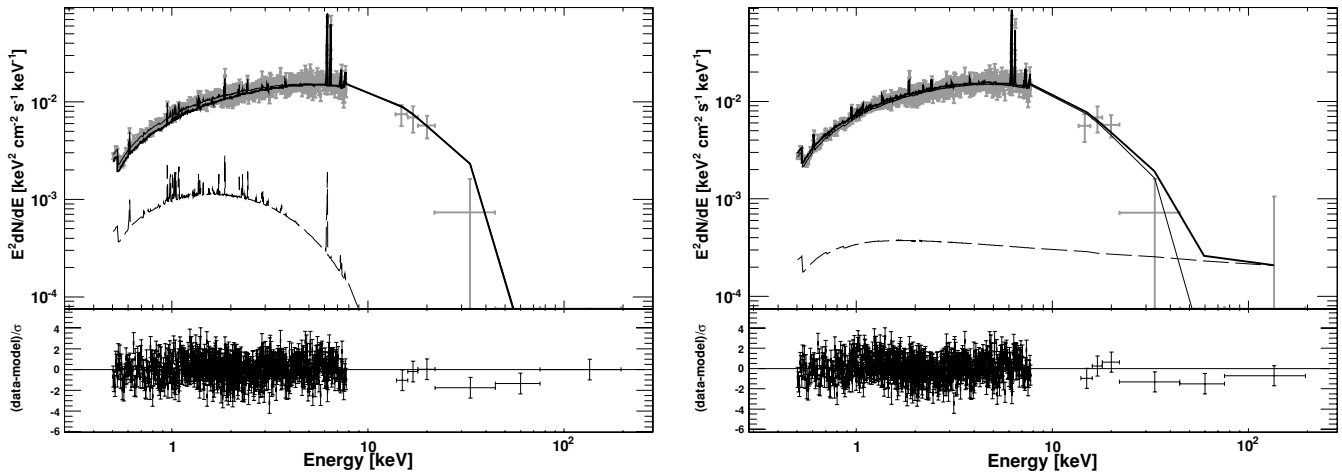

Figure 4. Left panel: spectrum of A401 fitted with the sum of two thermal models. Right panel: spectrum of A401 fitted with the sum of a thermal model and a power law.

additional parameters and is clearly not a better fit than the sum of two thermal models. Indeed the *F*-test yields a probability of 0.02 and 1.7×10^{-6} for the power law and the additional thermal model, respectively, of being spurious. For this reason, we believe that the sum of two thermal models is a more adequate representation of the *XMM-Newton*/BAT data set and we report its best-fit parameters in Table 3.

Since no spectral index for the radio emission is available in the literature, we adopt a value of $\alpha = 2.0$. Using a power law with a photon index of 2.0, we derive that the 99% CL upper limit on the non-thermal component in the 50–100 keV band is 2.2×10^{-13} erg cm^{-2} s^{-1}. As a final note, the brightest point source in the *XMM-Newton* 10′ region is located at R.A.(J2000) = 02:59:05.5 and decl.(J2000) = 13:39:44.9. Its spectrum is very soft and consistent with a bremsstrahlung model with a temperature of 0.3 ± 0.1 keV. Its flux in the 2–10 keV band is 1.9×10^{-16} erg cm^{-2} s^{-1} and thus it is negligible when compared to the cluster signal in both the *XMM-Newton* and BAT bands.

3.3. Bullet Cluster

1E 0657-56 is a distant cluster ($z = 0.296$), originally detected in the *Einstein* survey (Tucker et al. 1995). *ROSAT* and ASCA have shown that the Bullet is one of the hottest ($kT = 17.4 \pm 2.5$ keV), and most massive cluster known (Tucker et al. 1998). The same data show that 1E 0657-56 is undergoing a major merger process. Liang et al. (2000a) found that 1E 0657-56 contains a very luminous radio halo whose surface brightness closely follows the X-ray one. Weak and strong lensing reconstructions of the Bullet cluster are one of the best evidence for the existence of dark matter (e.g., Clowe et al. 2004, 2006; Markevitch et al. 2004; Bradač et al. 2006). The *Chandra* high-resolution image of a bullet-like gas cloud moving in the cluster core with a bow shock front, gained 1E 0657-56 the name Bullet cluster (Markevitch et al. 2002). The average temperature they report ranges from 14 to 15 keV to more than 20 keV. Deeper *Chandra* observations showed that, away from the Bullet, the radio-halo peak is offset from the X-ray peak, which is centered on the region hosting the hottest gas (Govoni et al. 2004). The Bullet cluster was observed also with *XMM-Newton* (Zhang et al. 2004, 2006; Finoguenov et al. 2005) and *RXTE* (Petrosian et al. 2006). The latter determined that the spectrum of the Bullet cluster can be fit equally well by the sum of two thermal models or by the sum of a thermal and a power-law model. They also estimated that the equipartition value of the magnetic field intensity is ∼1.2 μG. 1E 0657-56 has a complex radio morphology. The diffuse radio halo detected by Liang et al. (2000a) has a flux density $S_R = 78$ mJ at 1.3 GHz with a spectral index $\alpha = 1.2$.

The combined *XMM-Newton* and BAT data can be successfully fit (χ^2/dof = 524.7/513) by a single-temperature thermal (APEC) model (see left panel of Figure 5). The best-fit temperature is $12.57^{+0.64}_{-0.65}$ keV while the abundance is $0.25^{+0.06}_{-0.08}$ solar. The temperature is in moderately good agreement with the values of $14.5^{+2.0}_{-1.7}$ keV and $14.8^{+1.7}_{-1.2}$ keV as observed by ASCA and *Chandra*, respectively (Liang et al. 2000b; Markevitch et al. 2002) and is contained well in the range of temperatures observed with *Chandra* (see above references). Following Petrosian et al. (2006), we added a power-law model to the fit. The fit improves ($\Delta\chi^2 \approx 23$ for two additional parameters, i.e., 4.4σ) and the best-fit temperature becomes $14.77^{+1.13}_{-0.72}$ keV (in agreement with ASCA and *Chandra* results), while the power-law index is $1.86^{+1.25}_{-0.14}$. This model fit is reported in the right panel of Figure 5. The non-thermal 20–100 keV flux is $3.4^{+1.1}_{-1.0} \times 10^{-12}$ erg cm^{-2} s^{-1}. These values are in good agreement with those reported by Petrosian et al. (2006). Moreover, recently Million & Allen (2009), using *Chandra*, reported the detection of non-thermal flux in the 0.6–7.0 keV band at a level of $0.95^{+0.10}_{-0.11} \times 10^{-12}$ erg cm^{-2} s^{-1}. From our analysis, we derive that the 0.6–7.0 keV power-law flux is $3.3^{+1.2}_{-1.1} \times 10^{-12}$ erg cm^{-2} s^{-1} and thus slightly brighter than their reported flux.

For the sake of completeness, we also tried to fit the spectrum of the Bullet cluster with the sum of two thermal models. The hot, most intense component, shows as before a temperature of $15.4^{+2.4}_{-1.5}$ keV and an abundance of $0.30^{+0.10}_{-0.08}$ solar. The second component displays a temperature of $1.1^{+0.4}_{-0.2}$ keV, an abundance compatible with zero and a 1–10 keV flux of $6.3^{+3.8}_{-2.1} \times 10^{-13}$ erg cm^{-2} s^{-1}. This fit is shown in the lower panel of Figure 5. Both fits represent a reasonable description of the data. The thermal plus power-law model is slightly worse (χ^2/dof = 501.7/511) than the sum of two thermal models (χ^2/dof = 499.9/510). However, inspection of Figure 5 shows that the thermal plus power-law model better explains the residuals at high energy, albeit the BAT data are not very significant above 50 keV. We also checked that leaving the inter-calibration between BAT and *XMM-Newton* free to vary (see Section 2.5) does not change the results presented here.

Finally, we also verified the contribution of point sources to the overall signal. We found that only two sources produce a signal comparable to the excesses seen here. The first one is a bright point sources locate southwest of the cluster core at a position R.A.(J2000) = 06:58:13.8 and decl.(J2000) = −55:59:20.6. Its spectrum can be fit by an absorbed bremsstrahlung model, where the absorption is compatible with the Galactic one and the temperature of the plasma is $3.9^{+13.1}_{-2.31}$ keV. The 1–10 keV flux is $2.90^{+1.01}_{-1.50} \times 10^{-14}$ erg cm^{-2} s^{-1}. The second one is located at R.A.(J2000) = 06:58:03.8 and decl.(J2000) = −56:01:13.1 and its spectrum can be fit with an absorbed power law where the absorption is in excess of the Galactic one with $N_{\rm H} = 9.3^{+7.7}_{-4.4} \times 10^{21}$ cm^{-2} and the photon index is $1.46^{+0.55}_{-0.31}$. When extrapolated to the 20–100 keV band the source flux is $5.0^{+1.0}_{-2.45} \times 10^{-13}$ erg cm^{-2} s^{-1}. It is thus clear that both sources cannot account for the observed signals, indeed their fluxes are a factor of ∼10 below the flux of the "cold" component and the non-thermal component seen in the spectral fits described above.

Moreover, we checked whether the results reported above might be connected to some residual background contamination in *XMM-Newton* which was not accounted for correctly in the extraction of the background spectrum from blank field observations. For this purpose, we extracted a background spectrum from a region of the *XMM-Newton* CCD which is the least contaminated by the cluster emission. Since the Bullet cluster is at moderately high redshift, this is possible. We also extracted the background spectrum from a region whose area was the same as that of the one used to extract the cluster emission and whose position is diametrically opposite to the cluster region with respect to the pointing direction (to ensure a similar effective area over the two regions). The analysis of the Bullet cluster spectrum using this background strategy confirms the above results. In particular, both the "cold" component and the non-thermal power law are confirmed and the derived fluxes are consistent with those reported above. Thus, we can exclude an instrumental origin for both components.

In order to understand whether both components co-exist, we tried a fit with a model which is the sum of two thermal components and a power law. Not surprisingly, this model produces a good fit to the data (χ^2/ndf = 498.1/508). All parameters, with the exception of the normalization of the "cold" component, are fully compatible and in good agreement with the parameters reported above. Indeed, from this best fit we derive that the cold component has now a 1–10 keV flux of $7.7^{+1.1}_{-7.7} \times 10^{-14}$ erg cm^{-2} s^{-1} and thus a factor of ∼10 below the flux derived from the fit using two thermal models only. Moreover, as the statistical uncertainty shows, this component is now compatible with zero at 90% confidence.

On the other hand, the parameters of the power-law component are robust with respect to the variation of the other parameters (see Figure 6). For this and all the other reasons explained above, we believe that the description of the cluster spectrum in terms of a single thermal model and a power law is the best and most reliable one. The parameters of this fit are reported in Table 3. Our analysis thus confirms the presence of a power-law component in the spectrum of the Bullet cluster as reported by Petrosian et al. (2006).

3.4. PKS 0745-19

Early *Einstein* and *EXOSAT* observations showed that PKS 0745-19 (also known as 4U 0739-19) is one of the largest cool core clusters known (Fabian et al. 1985; Arnaud et al. 1987; Edge et al. 1990; White et al. 1997). The ICM temperature as measured with ASCA and *ROSAT* (Allen et al. 1996; Pierre & Starck 1998; Peres et al. 1998) agrees well with that found with *BeppoSAX*, of about 8.3 keV (De Grandi & Molendi 1999, 2001, 2002). Chen et al. (2003), using *XMM-Newton* and *Chandra*, reported an enhanced diffuse X-ray emission in correspondence of bright radio lobes. They discuss the possibility of buoyant bubbles to explain the observed X-ray and radio emission. However, Dunn & Fabian (2006), using *Chandra* data, find "no clear" evidence of such radio bubbles. Ball et al. (1993) and Baum & O'Dea (1991) classify PKS 0745-19 as an amorphous radio source, displaying both a compact radio source (five times brighter than Perseus) and a diffuse emission. These unusual radio properties do not seem to be just the result of AGN activity, but the result of a merger and/or buoyant plumes. Baum & O'Dea (1991) report that the intensity of the diffuse flux at 5 GHz is 265 mJy, while the spectral index is $\alpha = -1.4$. For these values, the equipartition magnetic field is in the 20–50 μG range.

Our data point to a thermal origin of the hard X-ray emission. Indeed, the *XMM-Newton* and BAT spectra can be successfully modeled by a single-temperature thermal model (χ^2/dof = 610.5/581) with a temperature of $6.69^{+0.25}_{-0.27}$ keV and an abundance of $0.35^{+0.03}_{-0.03}$. However, adding a second thermal

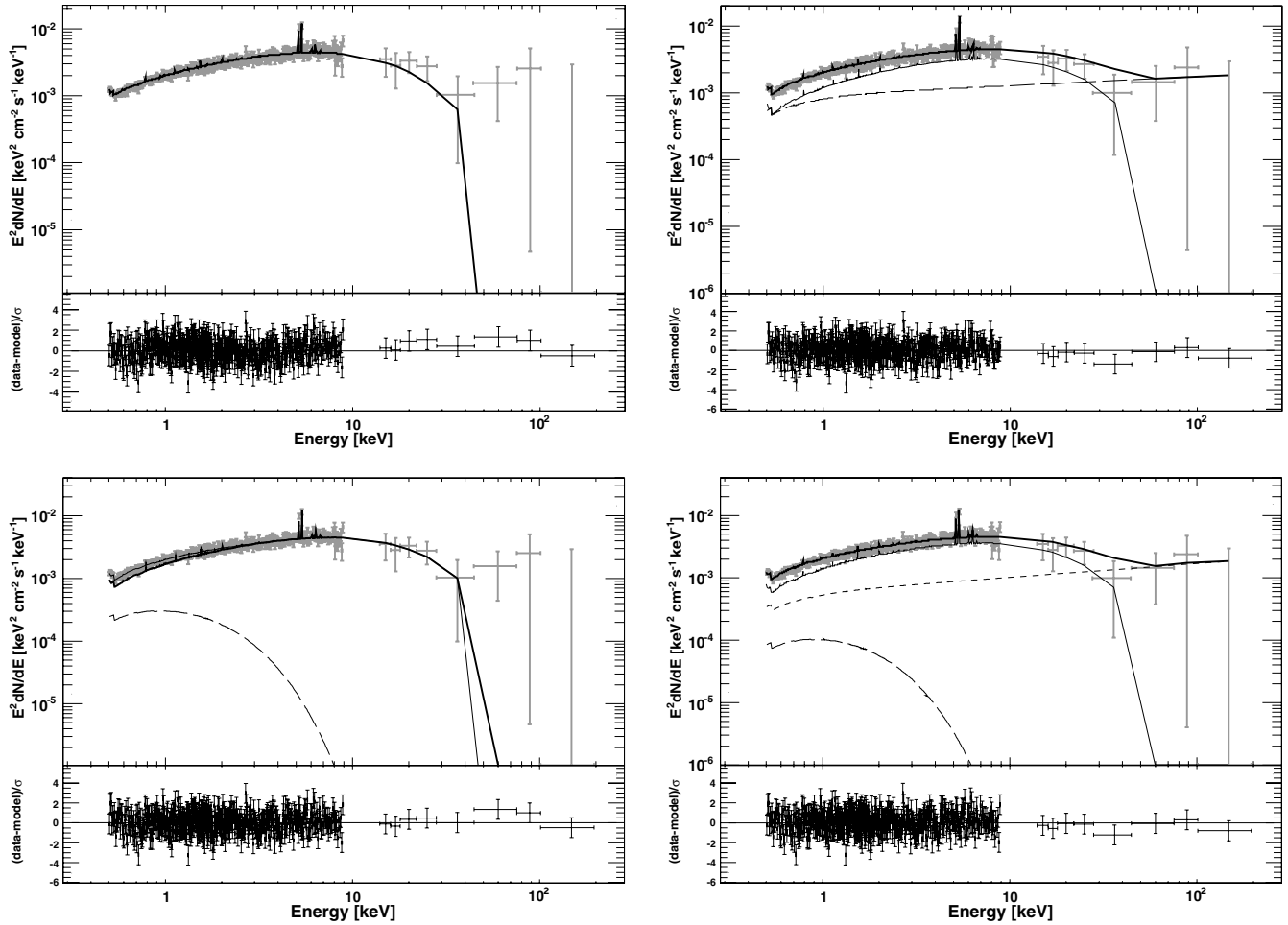

Figure 5. *XMM-Newton* and BAT data for the Bullet cluster fitted with (1) a single thermal model (upper left), (2) the sum of a thermal and a power-law model (upper right), (3) the sum of two thermal models (bottom left), and (4) sum of two thermal models (thin and long-dashed lines) and a power law (bottom right).

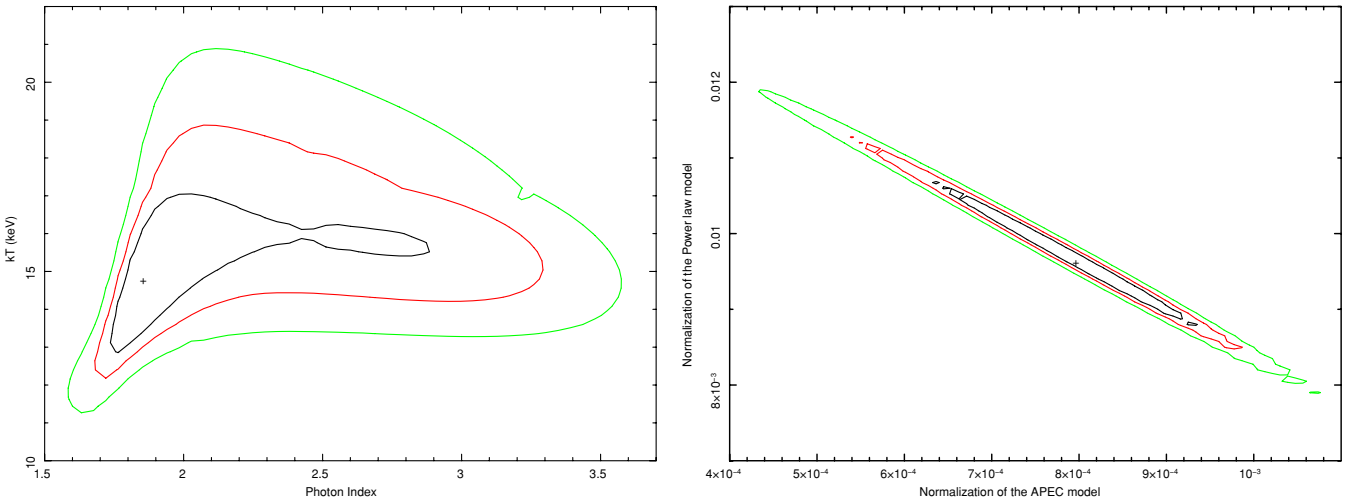

Figure 6. Contour (1σ, 2σ, and 3σ) plots of the parameters of the power-law component vs. the parameters of the most intense thermal component for the Bullet cluster.

(A color version of this figure is available in the online journal.)

component produces a noticeable improvement ($\Delta\chi^2 = 23.2$ for 3 additional degrees of freedom, corresponding to 5.0×10^{-5} chance). The hot most intense component now has a temperature of $7.96^{+0.68}_{-0.54}$ keV and an abundance of $0.40^{+0.05}_{-0.05}$, while the cold component displays a temperature of $2.16^{+1.08}_{-0.56}$ keV and an abundance of $0.31^{+0.05}_{-0.06}$. This fit is shown in the left panel of Figure 7. The temperatures observed here are consistent with those found by George et al. (2009) using *Suzaku*.

We also tried a fit with the sum of a thermal and a power-law model. The temperature and abundance of the thermal component are $7.53^{+0.27}_{-0.69}$ keV and $0.37^{+0.10}_{-0.07}$, while the photon

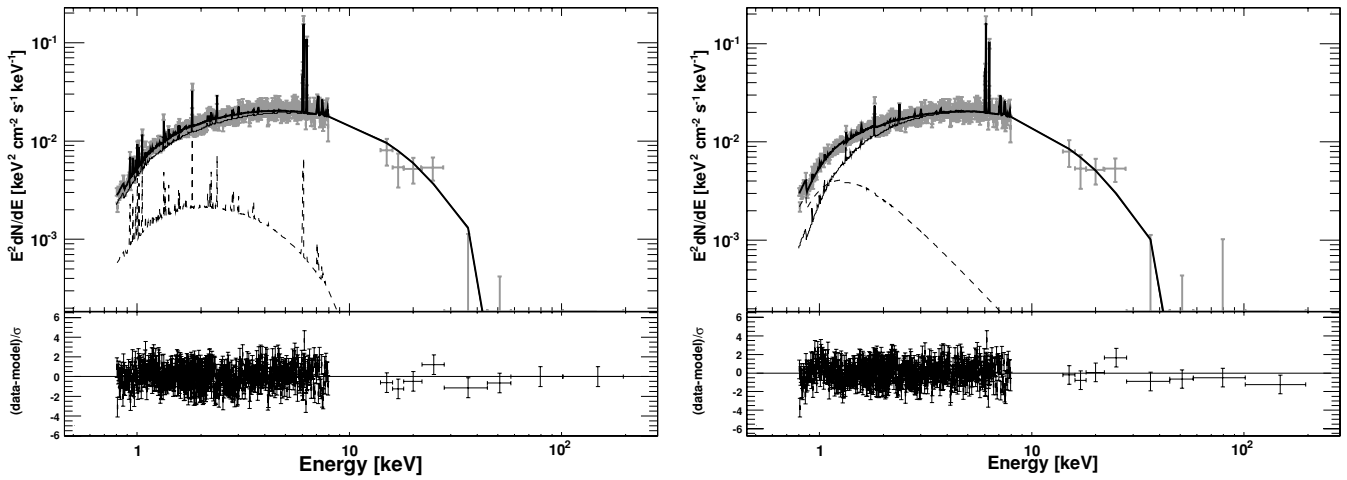

Figure 7. Left panel: spectrum of PKS 0745-19 fitted with the sum of two thermal models. Right panel: spectrum of PKS 0745-19 fitted with the sum of a thermal model and a power law (dashed line).

index of the power law is $4.39^{+0.79}_{-2.01}$. The improvement in χ^2 with respect to the single-temperature thermal model is $\Delta\chi^2 = 17$ for two additional parameters (corresponding to 0.2% chance). This fit is reported in the right panel of Figure 7. Nevertheless, given the very soft spectral index (which accounts for the "cold" component) and the marginal improvement in the fit statistics, we believe that the sum of two thermal models is a more reliable interpretation of the *XMM-Newton*/BAT data set. The parameters of this fit are thus summarized in Table 3.

Using the sum of two thermal models as a baseline spectral fit, we estimated the 99% CL to a non-thermal component in the 50–100 keV band using a power law with a photon index of 2.0. This is found to be 1.55×10^{-12} erg cm^{-2} s^{-1}. If instead a photon index of 2.4 is used, the upper limit in the 50–100 keV band becomes 1.10×10^{-12} erg cm^{-2} s^{-1}. Finally, the brightest point source in the *XMM-Newton* 10′ region is located at R.A.(J2000) = 07:47:19.0 and decl.(J2000) = −19:24:02.3. Its spectrum is very soft and consistent with a bremsstrahlung model with a temperature of 0.7 ± 0.3 keV. Its flux in the 2–10 keV band is 2.6×10^{-15} erg cm^{-2} s^{-1} and thus it is negligible when compared to the cluster signal in both the *XMM-Newton* and BAT bands.

3.5. A1795

A1795 is a compact and rich cluster with a strong cool core (e.g., Edge et al. 1992; Briel & Henry 1996; Markevitch et al. 1998; Tamura et al. 2001). It has been extensively observed with HEAO-1, *Einstein*, *EXOSAT*, *ROSAT*, *BeppoSAX*, *XMM-Newton*, *Chandra*, and *RXTE* (e.g., Kowalski et al. 1984; Rhee & Latour 1991; Edge et al. 1990; Arnaud et al. 1991, 2001; Markevitch et al. 1998; Sanders et al. 2000; Nevalainen et al. 2004; Revnivtsev et al. 2004; Vikhlinin et al. 2005, and references therein). EGRET was also used to set an upper limit to the γ-ray emission from the ICM (above 100 MeV; Reimer et al. 2003). Outside the cool region, the average temperature is of 6–7 keV (e.g., Arnaud et al. 2001). A1795 is a relaxed cluster, although there is evidence that the central brightest galaxy is not at rest (Hill et al. 1988) and that there is inner gas sloshing in the potential well (Markevitch et al. 2001; Ettori et al. 2002). No hard X-ray excess has ever been reported for this cluster. Fabian et al. (2001) discovered a 40″ long cold filament in the core of the cluster, coincident with an Hα filament. The straightness of the filament indicates that the ICM is not very turbulent. A1795 has two X-ray dim regions (e.g., Fabian et al. 2001; Ettori et al. 2002) in correspondence of radio bubbles (Dunn et al. 2005). The radio morphology is dominated by two radio regions (Guthrie 1974; Owen 1975; Dagkesamanskii et al. 1982; Alikberov et al. 1983; Burns 1990; Owen et al. 1993; Owen & Ledlow 1997; Dunn et al. 2005), but there is no strong evidence for a large-scale radio halo (Hanisch 1982). Ge & Owen (1993) report Faraday rotation measurements of the small central radio galaxy 1346+268. They conclude that the associated magnetic field must be >20 μG and that it is most likely associated with the ICM rather than with the small radio source.

Using the parameters of the surface brightness reported by Briel & Henry (1996; e.g., core radius of 5.′15 and $\beta = 0.93$), we derive that our standard selection region of 10′ radius (in *XMM-Newton*) includes 97%–99% of the cluster emission. The *XMM-Newton* and *Swift*/BAT data are best modeled (χ^2/dof = 892.1/1275) by a single thermal model with a temperature of $4.82^{+0.10}_{-0.11}$ keV and an abundance of $0.45^{+0.04}_{-0.04}$. Our results are in good agreement with that of Tamura et al. (2001). Given the very good χ^2, adding other models (or free parameters) does not improve the fit. Thus, we believe that the single thermal model is a good representation of the *XMM-Newton*/BAT data set. This fit is shown in the left panel of Figure 8.

As a final note, the field of A1795 contains a bright AGN located at R.A.(J2000) = 13:48:35.2 and decl.(J2000) = 26:31:08.9, which lies less than 3′ from the cluster core. This source is the Seyfert 1 galaxy 1E 1346+26.7. In *XMM-Newton*, it exhibits an unabsorbed power-law spectrum with a photon index of 2.34 ± 0.04 and a 2–10 keV flux of $8.7(\pm0.1) \times 10^{-13}$ erg cm^{-2} s^{-1} (approximately 1% of the cluster's signal in that band). When extrapolated to the 15–55 keV band, the AGN flux becomes $3.7(\pm0.1) \times 10^{-13}$ erg cm^{-2} s^{-1} and thus still a factor of ∼5 below the cluster emission in that band (see Table 3). We checked that the results reported above do not change if the AGN emission is properly modeled (e.g., with the parameters of the AGN power law allowed to vary within their errors) in the joint fit to the overall cluster's spectrum. However, when computing the (50–100 keV) 99% CL upper limit on the non-thermal component (using a power law with a photon index of 2.0), we derive that this is 1.57×10^{-12} erg cm^{-2} s^{-1} if the AGN contribution is not taken into account, or 1.06×10^{-12} erg cm^{-2} s^{-1} if it is. We will thus use this second upper limit in Table 4.

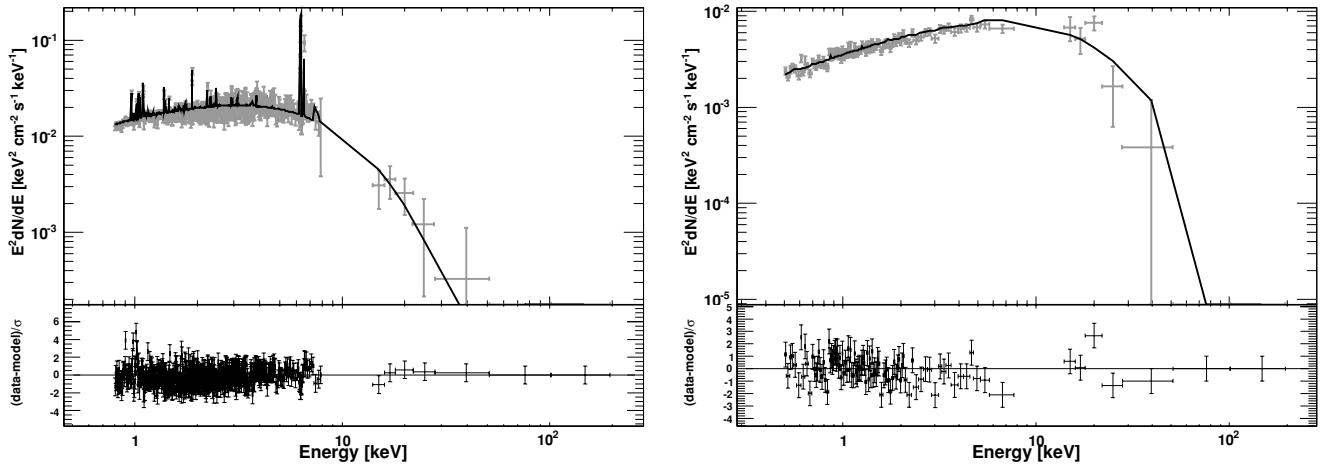

Figure 8. Left panel: spectrum of A1795 fitted with a single-temperature thermal model. Right panel: spectrum of A1914 fitted with a single-temperature thermal model.

Table 4
Non-thermal Emission from Combined *XMM-Newton* and BAT Data

Name	$F_{50-100\,\mathrm{keV}}$[a] (10^{-12} erg cm^2 s^{-1})	B[b] (μG)
A85	<2.51	∼0.6
A401	<0.22	∼0.4
Bullet	$1.58^{+0.43}_{-0.47}$	∼0.16
PKS 0745-19	<1.6	∼0.5
A1795	<1.38	/
A1914	<1.08	∼0.3
A2256	<0.19	∼0.6
A3667	$2.98^{+4.17}_{-0.73}$	/
A2390	<0.25	∼0.8

Notes.
[a] The flux has been estimated using a power-law spectrum with a photon index of 2.0 in the 1–200 keV energy band. Upper limits are 99% CL while errors are 90%% CL.
[b] In order to compute the intensity of the magnetic field, we used the radio data listed in Section 2. When α was not available, we adopted $\alpha = 2$.

3.6. A1914

A1914 is a regular and smooth galaxy cluster. It has been observed with *ROSAT* (Ebeling et al. 1996; Buote & Tsai 1996; Böhringer et al. 2000), ASCA (White 2000; Ikebe et al. 2002), and *Chandra* (Govoni et al. 2004; Baldi et al. 2007). By means of a comparison of X-ray and radio maps, Govoni et al. (2004) discuss a possible merger scenario. Baldi et al. (2007) report an average ICM temperature of 9.20 ± 0.39 keV. A1914 is known to host a very steep radio source (Kulkarni et al. 1990) and a radio halo (Giovannini et al. 1999; Kempner & Sarazin 2001; Bacchi et al. 2003). The point sources make the estimation of the diffuse flux density difficult. We adopt the value of $S_R = 64$ mJ at 1.4 GHz and the reported spectral index of $\alpha = 1.8$ from Bacchi et al. (2003). The equipartition magnetic field is 0.5 μG.

The *Swift*/BAT spectrum can be fit by a bremsstrahlung model with a plasma temperature of $7.30^{+3.18}_{-2.01}$ keV. The combined *XMM-Newton–Swift*/BAT data set can be successfully modeled (χ^2/dof = 355.1/351) with a single-temperature thermal model (see the right panel of Figure 8). The best-fit temperature and metallicity are $11.14^{+1.13}_{-1.09}$ keV and 0.19 ± 0.14 solar, in agreement with the studies mentioned above. Given the good χ^2 adding other models to the single thermal model does not improve the fit results. The 99% CL upper limit on the 50–100 keV non-thermal flux, evaluated with a power law with a photon index of 2.0, flux is 1.08×10^{-12} erg cm^{-2} s^{-1}. If we use a power law with a photon index of 2.8 (in line with the radio photon index) then the upper limit is much tighter and it becomes 4.60×10^{-14} erg cm^{-2} s^{-1}. However, this upper limit to the non-thermal flux in the (BAT) 50–100 keV band, is entirely driven by the *XMM-Newton* signal below 2 keV. Indeed, if we repeat the same process described above, but using only *Swift*/BAT data, then the 99% CL upper limit (using a photon index of 2.8) is 1.16×10^{-12} erg cm^{-2} s^{-1} and thus in line with the one computed using a power law with a photon index of 2.0 and the entire *XMM-Newton*/BAT data set. We thus believe that this (e.g., 1.08×10^{-12} erg cm^{-2} s^{-1}) is a more reliable upper limit for the 50–100 keV band.

3.7. A2256

A2256 is a rich cluster at a redshift of 0.0581, bright both at radio and X-ray energies (e.g., Bridle & Fomalont 1976; Briel et al. 1991; Henriksen 1999). It has been studied several times at X-rays and the disturbed morphology of the X-ray temperature map indicates a cluster in an advanced merging stage (e.g., Molendi et al. 2000). A2256 is one of those clusters for which a claim of significant detection of non-thermal emission has been reported. Indeed, Fusco-Femiano et al. (2000), using data from *BeppoSAX*, reported the detection of a hard X-ray excess at the 4.6σ level. The 20–80 keV flux of this excess is 1.2×10^{-11} erg cm^{-2} s^{-1}. Rephaeli & Gruber (2003), using *RXTE* data, reported the detection of an hard X-ray excess whose 20–80 keV flux is $4.3^{+5.7}_{-4.0} \times 10^{-12}$ erg cm^{-2} s^{-1} (errors are 90% CL) and thus a factor of ∼3 fainter than the one reported by Fusco-Femiano et al. (2000), but marginally consistent with it. A re-analysis by Fusco-Femiano et al. (2005) confirmed the *BeppoSAX* detection (at 4.8σ) albeit at a lower 20–80 keV flux of $8.9^{+4.0}_{-3.6} \times 10^{-12}$ erg cm^{-2} s^{-1}. In the radio band, A2256 displays an extremely complex morphology consisting of a bright relic and a fainter steep-spectrum radio halo located in the cluster center (Clarke & Ensslin 2006). The total flux density of this radio halo is 100 mJy at 610 MHz (Rengelink et al. 1997) and 103.4 mJy at 1369 MHz (Clarke & Ensslin 2006), while the spectral index is $\alpha = 1.8$.

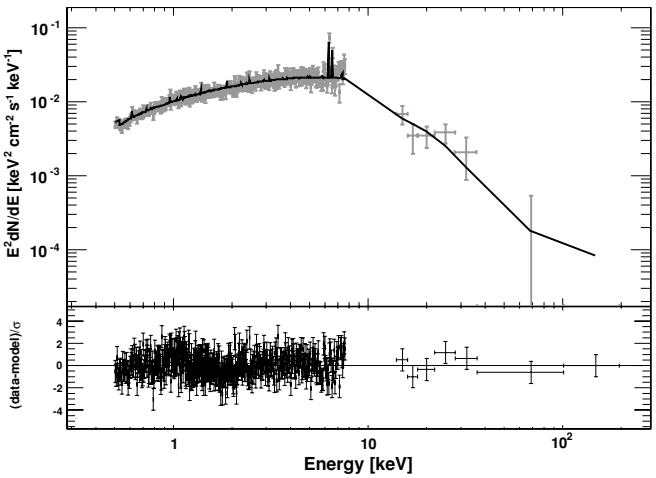

Figure 9. Spectrum of A2256 fitted with a single-temperature thermal model.

The BAT data alone are fit well by a bremsstrahlung model with a temperature of $9.8^{+7.7}_{-3.8}$ keV. Adopting the values reported by Briel et al. (1991) (e.g., core radius of 4.83 ± 0.17 arcmin and $\beta = 0.756 \pm 0.013$), we derive that selecting photons within 10′ of the core includes ∼95% of the cluster's emission. The joint *XMM-Newton*–BAT data set is fit well (χ^2/dof = 445.6/445) by a single thermal model with a temperature of $8.84^{+0.66}_{-0.61}$ keV and an abundance of 0.22 ± 0.06. The best fit is shown in Figure 9 while the parameters are reported in Table 3. Henriksen (1999) found out that the best spectral model reproducing the *RXTE*/ASCA data sets, for A2256, is produced by the sum of two thermal models. In that work, the hot and the cold components have a temperature of ∼7 keV and ∼1 keV, respectively. Following his example, we added a second thermal model to the fit keeping the abundance of this additional component fixed at 0.3 (allowing this parameter to vary does not change the results). The best-fit temperature of the additional component is 1.08 ± 0.39 keV in good agreement with the results of Henriksen (1999) while the temperature and abundance of the hot component did not vary appreciably. However, the improvement in $\Delta\chi^2$ is 2.5 for two additional parameters and thus not significant (i.e., the probability that the improvement was obtained by chance is ∼0.3). We thus believe that the single-temperature thermal model discussed above represents the best description of the *XMM-Newton*–BAT data set.

The 99% CL upper limit on the 20–80 keV non-thermal flux is 6.1×10^{-12} erg cm^{-2} s^{-1}. The upper limit derived by our analysis is lower than the hard X-ray excess claimed by Fusco-Femiano et al. (2005). Even using BAT data alone, the 99% upper limit in the 20–80 keV band is 4.6×10^{-12} erg cm^{-2} s^{-1} and thus inconsistent with the *BeppoSAX* result (but not with the *RXTE* one). In our band (50–100 keV) the upper limit, derived from the joint data set, is 2.41×10^{-12} erg cm^{-2} s^{-1}. If instead of a power law with an index of 2.0, we use a power law with a photon index of 2.8 (the value of the radio halo) the 50–100 keV upper limit on the non-thermal emission would be 1.97×10^{-13} erg cm^{-2} s^{-1}.

3.8. A3627

A3627, known also as Norma cluster at $z = 0.015$, is a nearby massive cluster located behind the Milky Way in the core of the Great Attractor and discovered as an important component of the local large-scale structure by Kraan-Korteweg et al. (1996). It is a very rich cluster with a mass comparable to that of Coma and Perseus (i.e., $>2 \times 10^{15}$ $M_\odot$). Early X-ray observations with *ROSAT* and ASCA show that the cluster is not spherically symmetric and has a strong temperature gradient ($\Delta kT \sim 3$ keV) in the direction of the elongation (Boehringer et al. 1996; Tamura et al. 1998). This fact indicates that A3627 is in the stage of a major merger. This cluster also exhibits spectacular head–tail radio-galaxies (e.g., Sun et al. 2010) which are galaxies likely traveling at high velocities through the ICM (see, e.g., Sarazin 1988). At the cluster center, PKS 1610-608 displays, in radio, two powerful jets and two lobes whose surface brightness peaks respectively at ∼1′ and ∼5′ away from the galaxy. Jones & McAdam (1996) find that the intensity of the magnetic field, derived assuming equipartition, is ∼15 μG at the position of the jets and ∼5 μG at the lobes.

Considering the values for the surface brightness reported by Boehringer et al. (1996; e.g., core radius of 9.′95 and β = 0.55) and Figure 1, it is clear that Norma should be detected, by BAT, as an extended source. However, its elongation (e.g., not being spherical symmetric) does not allows us to determine a priori the expected likely flux suppression in BAT. This is made even more complex by the presence of a nearby AGN (IGR J16119-6036) which is detected at a significance of ∼10σ by BAT (Cusumano et al. 2010). This AGN is located at ∼20′ away from the BAT centroid of Norma and the two sources appear separated. Figure 10 shows the contours of the surface brightness of Norma (as derived from *ROSAT*-PSPC observations) superimposed on the BAT significance map for that region. It is clear from the *ROSAT* contours that Norma extends likely all the way to the nearest point-like source (IGR J16119-6036). We should thus expect a contamination of the cluster thermal emission in the BAT spectrum of IGR J16119-6036. This would imply that BAT detects the Norma cluster as an extended source. We started fitting the BAT data alone for the Norma cluster with a bremsstrahlung model. The fit is acceptable (χ^2/dof = 14.4/14) and the best-fit temperature is $11.6^{+6.2}_{-3.3}$ keV. Next, we extracted *Swift*/XRT data for IGR J16119-6036 and fitted them together with the BAT data for this source. The results are reported in Figure 11. When using a single absorbed power law (which fits the XRT data alone well), the fit to the XRT–BAT data set is unacceptable with χ^2/dof = 31.5/16 and leaves residuals (as can be seen in the left panel of Figure 11) in the BAT band. We then added a bremsstrahlung model (only for the BAT, since XRT detects IGR J16119-6036 as point source) to the AGN power law, to check whether the BAT spectrum is contaminated by the thermal emission from the Norma cluster. The fit with this model is good (χ^2/dof = 12.1/14) and the photon index of the power law is 1.67 ± 0.16 while the temperature of the thermal model is 12.3 ± 4.2 keV. The temperature is in good agreement with the temperature of the Norma cluster (as measured with BAT) reported above and thus we conclude that there is significant contamination, particularly below 50 keV, of cluster's emission in the BAT spectrum of IGR J16119-6036. This also means that BAT detects the Norma cluster as an extended source.

Given the finding that BAT "resolves" Norma, it becomes difficult to determine how much flux has been suppressed by the mask and such detailed analysis will be left to a future paper. For this reason, instead of providing a joint fit to *XMM-Newton* and BAT, we perform two separate spectral fits. The BAT data, as already described, are shown in the left panel of Figure 12 and are well fit with a bremsstrahlung model with a temperature of $11.6^{+6.2}_{-3.3}$ keV. The *XMM-Newton* data (extracted around 10′

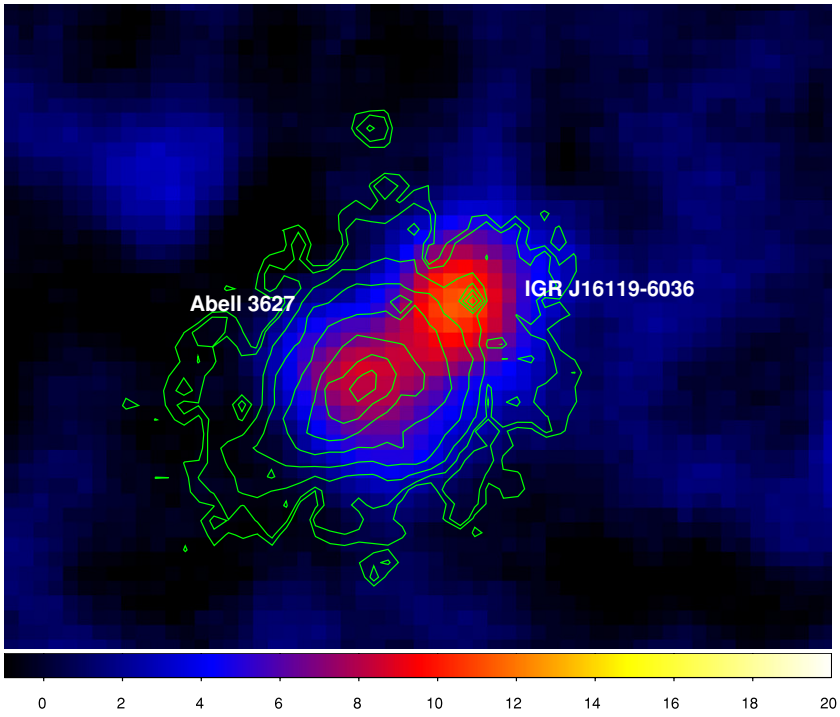

Figure 10. Contours of the surface brightness of the Norma cluster, as derived from *ROSAT*-PSPC observations, superimposed on the *Swift*/BAT significance map. (A color version of this figure is available in the online journal.)

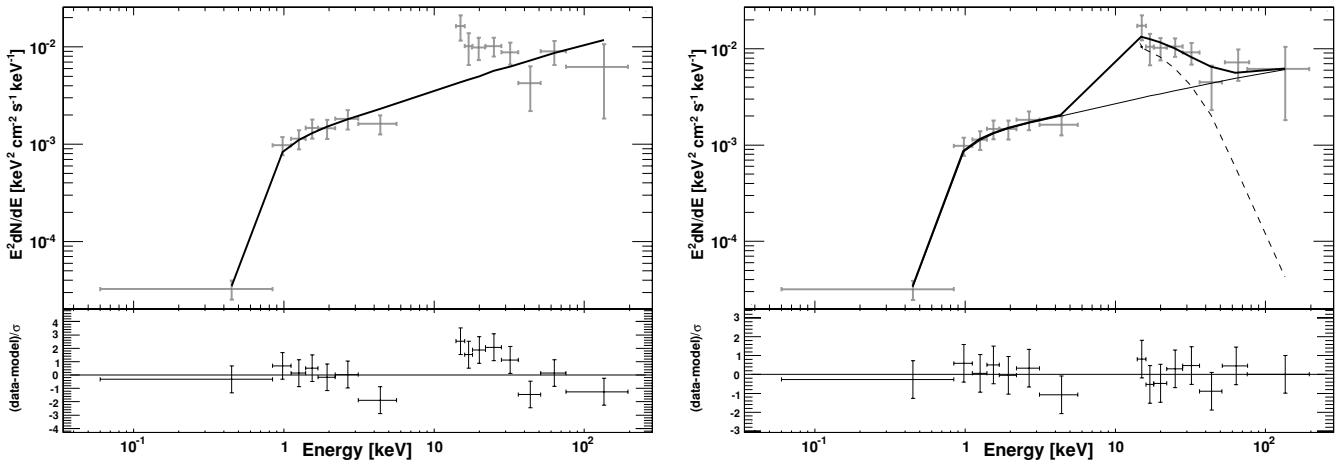

Figure 11. Left panel: XRT and BAT spectrum of IGR J16119-6036 fitted with a power law. Right panel: XRT and BAT spectrum of IGR J16119-6036 fitted with the sum of a power law and a thermal model (the latter only for the BAT data).

from the BAT centroid) are well fit (χ^2/dof = 402.6/377) by an APEC model with a temperature of $5.53^{+0.26}_{-0.23}$ keV and an abundance of $0.26^{+0.06}_{-0.03}$. This spectrum is shown in the right panel of Figure 12. Clearly, this analysis points to a difference in the temperature of the plasma as measured with the two instruments. This piece of evidence[14] would point toward the existence of regions of hot gas in the Norma cluster. While spatially resolved spectroscopy is not available for this cluster, both Boehringer et al. (1996) and Tamura et al. (1998) find that for some regions of the cluster temperatures as high as 7–10 keV might exist, thus in agreement with the BAT detection. For this cluster, we report in Table 3 the parameters of the best fit to the BAT data alone. Since it is resolved by BAT, part of its >15 keV flux is lost in the background and an upper limit to the non-thermal emission is not computed.

3.9. A3667

A3667 is a cluster at $z = 0.055$ discovered by HEAO (Piccinotti et al. 1982). *ROSAT* revealed that A3667 is a dynamically interacting system with a significant X-ray emission associated with a group of galaxies which is likely merging with the cluster. *ROSAT* measured for the cluster an average temperature of ∼6.5 keV (Knopp et al. 1996). Its dynamically complex structure has been investigate by Vikhlinin et al. (2001) using *Chandra*, revealing that the dense cool core is moving with high velocity through the hotter, less dense, surrounding gas, creating a cold front. Vikhlinin et al. (2001) estimated the intensity of the magnetic field, in the vicinity of the shock

[14] The *XMM-Newton* and BAT temperature are still compatible with each other within $\sim 2\sigma$.

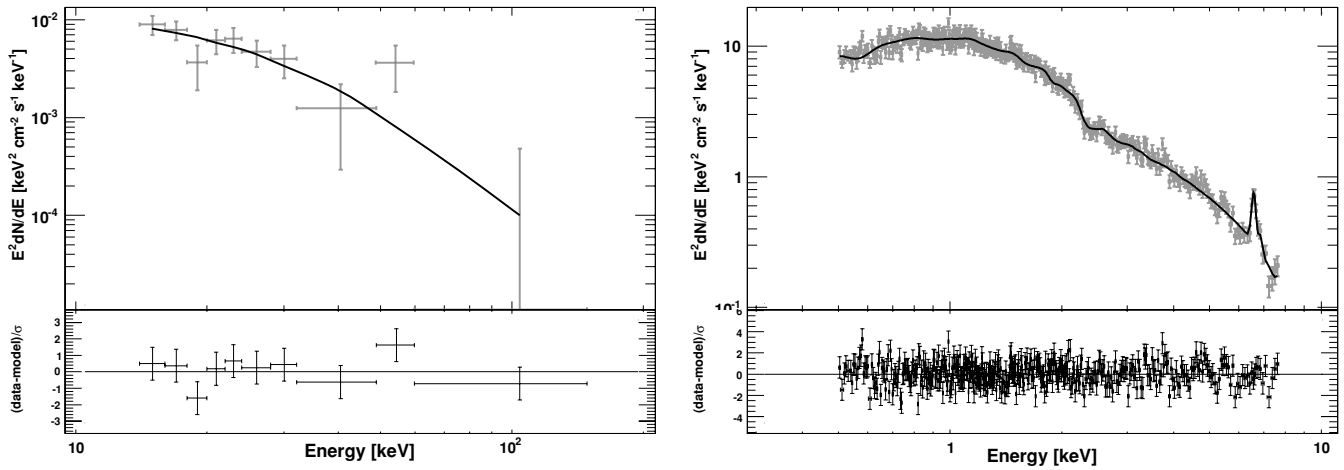

Figure 12. Left panel: BAT data for A3627 fitted with a bremsstrahlung model. Right panel: *XMM-Newton* data for A3627 fitted with a single thermal model.

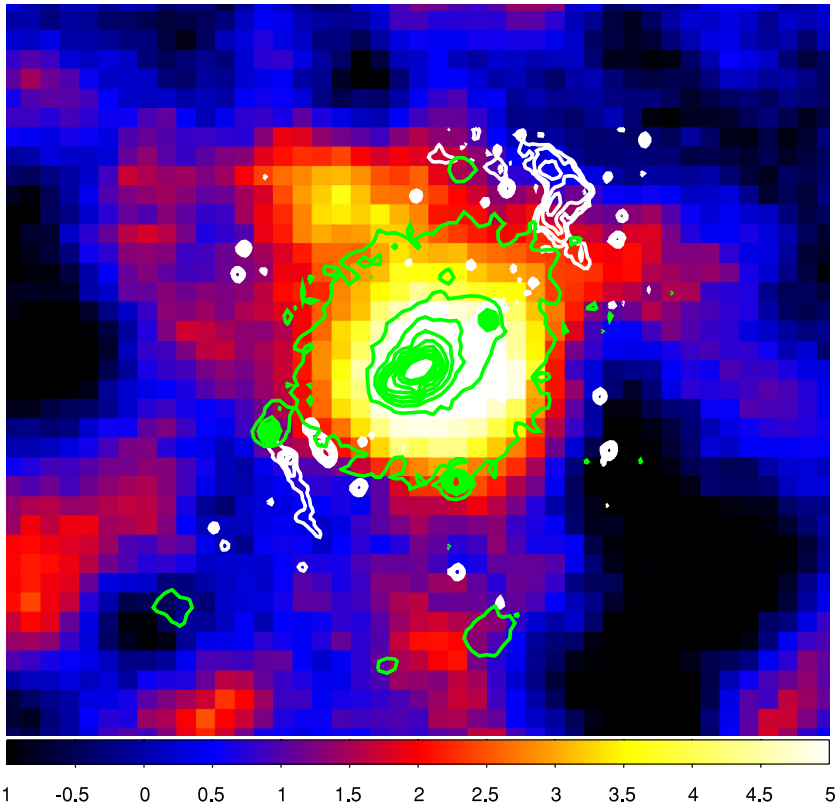

Figure 13. BAT significance map of A3667 with superimposed X-ray contours from the *ROSAT*-PSPC (green) and radio 843 MHz SUMSS contours (white).
(A color version of this figure is available in the online journal.)

region, to be $B \sim 10\ \mu$G. The magnetic field near the cold front is expected to be stronger and to have a very different structure compared to the bulk of the ICM. These peculiar characteristics make A3667 a good candidate for the detection of a hard X-ray excess of non-thermal origin. This component has, indeed, been reported in hard X-ray spectrum measured by *BeppoSAX* (Fusco-Femiano et al. 2001).

A3667 was recently studied in detail by Nakazawa et al. (2009) using data from *Suzaku*. When modeling the XIS (0.7–8.0 keV) and HXD (15–40 keV) spectra, they found that a single thermal model fails to explain the hard X-ray data and that another component is needed. This is required to be a very hot thermal component with $T = 19.2^{+4.7}_{-4.0}$ keV or a power law with an index of $1.39^{+0.10}_{-0.17}$ (Nakazawa et al. 2009).

Figure 13 shows the BAT significance map with superimposed contours from *ROSAT* (X-rays) and SUMSS (radio). It is clear that the BAT detection is associated with the core of the cluster and it is not compatible with as coming from the radio relic which lies $\geqslant 12'$ northwest of the BAT centroid. The BAT spectrum (reported in Figure 14) shows that A3667 is indeed an interesting cluster. A simple bremsstrahlung model fits the data well and the best-fit temperature is $18.7^{+22.6}_{-9.3}$ keV which is unusually high even for BAT and in agreement with that found by *Suzaku*. Adopting the values for the surface brightness reported

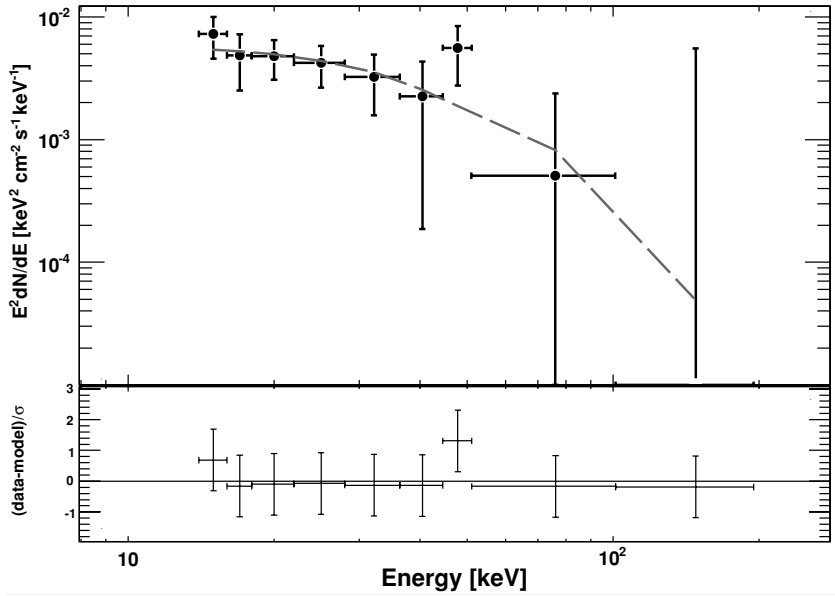

Figure 14. BAT spectrum of A3667. The dashed line is the best-fit thermal model with a temperature of $18.7^{+22.6}_{-9.3}$ keV.

by Boehringer et al. (1996; e.g., core radius of 2.′97 and $\beta = 0.55$), we derive that our standard selection, in *XMM-Newton*, of photons within 10′ includes ∼85%–95% of the cluster's emission. When analyzing jointly *XMM-Newton–Swift*/BAT data, we find that a single thermal model yields a best-fit temperature of 5.68 ± 0.19 keV and an abundance of 0.21 ± 0.04 solar. This fit is reported in the upper panel of Figure 15. It is apparent that this fit leaves unsatisfactory residuals at high energy. We then tried adding a second thermal component. The fit improves and the two thermal components show a temperature of $13.5^{+6.9}_{-2.2}$ keV and $3.9^{+0.8}_{-2.1}$ keV, respectively. The *F*-test shows that the probability of the second component being spurious is only 4.86×10^{-6}.

An equally good fit can be obtained with the sum of a thermal and a power-law model. In this case, the best-fit temperature is 5.91 ± 0.05 keV and the photon index is $1.83^{+0.36}_{-0.34}$. Again the *F*-test shows that the probability of the second component being spurious is very low, 3.46×10^{-6} (e.g., the significance of the model is ∼4.6σ). The power-law flux in the 10–40 keV band is $4.91^{+0.30}_{-2.00} \times 10^{-12}$ erg cm^{-2} s^{-1}, a factor of ∼10 fainter than the one reported by Nakazawa et al. (2009).

The two models discussed here produce the same result in term of goodness of fit and point to the existence of a very hot region with a temperature of ∼13 keV (as the BAT data alone testify). On a purely statistical basis, the model with lesser parameters should be chosen (e.g., the thermal plus power-law model). However, on a physical basis it is difficult to understand whether this excess is due to a hot component (as seen in other cases) or due to a truly non-thermal power-law-like one. We believe that the hot component is the more realistic hypothesis for several reasons: first the temperature of this component is not unusually high for massive and merging galaxy clusters. Second, A3667 is known to have radio relics, but not a central radio halo (Rottgering et al. 1997). Since the BAT centroid (see Table 1) is compatible with the cluster core and not with the relic, this renders the interpretation of the hard X-ray excess as being non-thermal unlikely. In support of the thermal interpretation of the hard X-ray excess, we note that the BAT centroid coincides with the hottest region ($kT \geqslant 8$ keV) as found with *XMM-Newton* (Briel et al. 2004). For this reason, we decided to report the sum of the two thermal models in Table 3.

In order to exclude that this hard X-ray excess originates from one of the point sources, we extracted the spectrum of the brightest X-ray sources located in the cluster field. Among all of them the brightest is the source positioned at R.A.(J2000) = 303.14908 and decl.(J2000) = −56.89704 with an uncertainty of 3″. The *XMM-Newton* spectrum is consistent with a simple power law with an index of 1.73 ± 0.20. Its flux extrapolated to the 10–40 keV band is $2.68^{+1.27}_{-0.70} \times 10^{-13}$ cm^{-2} s^{-1}. Since this flux is a factor of >10 fainter than the hard X-ray excess, we can exclude that the hard X-ray excess is caused by point-like sources. We thus conclude, partly confirming the result of Nakazawa et al. (2009), that our data require a hot component ($kT = 13.5^{+6.9}_{-2.2}$ keV) or a power law with a photon index of $1.83^{+0.36}_{-0.34}$. In this last case, the 50–100 keV non-thermal flux is $2.98^{+4.17}_{-0.73} \times 10^{-12}$ erg cm^{-2} s^{-1}.

Finally we note that, as can be seen from Figure 13, there is a small ∼3.5σ fluctuation in the BAT map ∼12′ northeast of the cluster core. However, we remark that until the 5σ threshold is exceeded, this has to be considered a statistical fluctuation. Indeed, the probability of observing a pure $\geqslant$3.5σ statistical fluctuation in the BAT map is quite large (i.e., 2.3×10^{-4}) leading[15] to a total of ∼6700 statistical fluctuations. Moreover, no known AGN or (bright) X-ray sources are reported within 5′ of this fluctuation and inspection of all the available X-ray data (*XMM-Newton*, *Swift*/XRT, *ROSAT*, etc.) did not reveal any potential candidate that might be the counterpart of this sub-threshold object. We thus believe this to be just a statistical fluctuation.

3.10. A2390

A2390 is a rich lensing galaxy cluster with a massive cool core (e.g., Pierre et al. 1996). It is among the 10 X-ray brightest galaxy clusters at redshift larger than 0.18 (e.g., Ebeling et al. 1996). It has been observed with HEAO-1 and 2 (Johnson et al. 1983; Kowalski et al. 1984; Wood et al. 1984; Ulmer et al. 1986), *Einstein* (McMillan et al. 1989), *ROSAT* (Pierre et al. 1996; Ebeling et al. 1996; Pierre & Starck 1998; Rizza et al. 1998;

[15] The probability of observing a fluctuation has to be multiplied by the number of pixels in the BAT map (i.e., 2.9×10^7; Segreto et al. 2010).

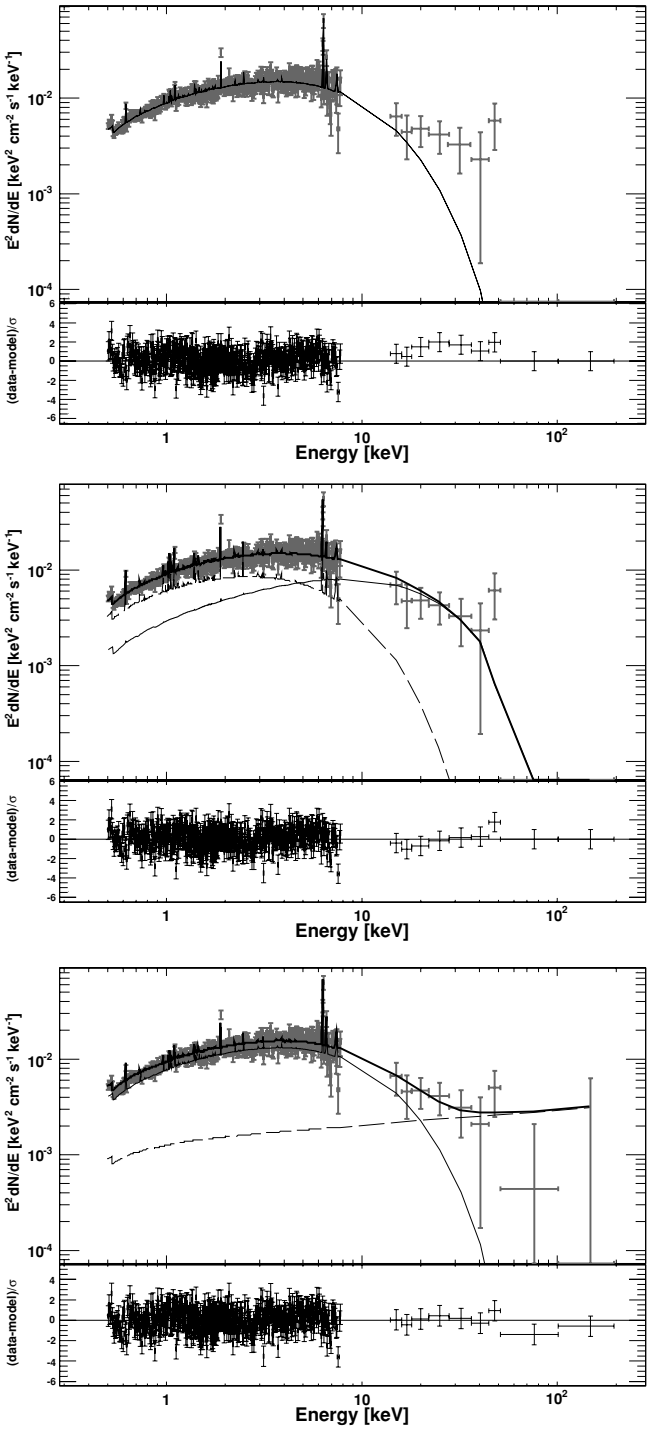

Figure 15. *XMM-Newton* and BAT data for A3667 fitted with (1) a single thermal model (top), (2) the sum of two thermal models (middle), and (3) the sum of a thermal and a power-law model.

Böhringer et al. 2000), ASCA (Mushotzky & Loewenstein 1997; Boehringer et al. 1998; White 2000), and *BeppoSAX* (Ettori et al. 2001). *Chandra* showed that A2390 is experiencing a minor merger event (see, e.g., Allen et al. 2001; Vikhlinin et al. 2005; Baldi et al. 2007). Outside the cooling region, the average temperature is 11.5 keV (Allen et al. 2001). A2390 has a small (less than 2′) irregular radio halo, most likely related to the central AGN (like the mini-halo of Perseus cluster; Bacchi et al. 2003). Its flux density is 63 mJ at 1.4 GHz and the equipartition magnetic field was estimated to be 1.3 μG (Bacchi et al. 2003). Using the model of the surface brightness profile of A2390 determined with *Chandra* (e.g., see Allen et al. 2001, for details), we derive that selecting photons in *XMM-Newton* within a radius of 10′ of the core includes virtually all of the cluster's emission.

There are two bright X-ray sources located within the selection region. Their coordinates are respectively R.A. (J2000) = 21:53:40.7 and decl.(J2000) = 17:44:13.8 for the brightest source R.A. = 21:53:34.6 and decl. = 17:36:26.8 for the dimmer one. Crawford et al. (2002) conducted follow-up observations of all sources detected with *Chandra* in the field of A2390. The sources reported above correspond to the sources A20 and A19 in their paper. Both these sources are AGNs with A19 being a Seyfert 2 galaxy at $z = 0.305$ and A19 a QSO at $z = 1.6750$. The spectrum of A20 is fit well by an absorbed power law with column density of $N_{\rm H} = 6.9^{+0.55}_{-0.30} \times 10^{21}$ cm^{-2} and a photon index of $1.52^{+0.44}_{-0.24}$. Its flux in the 2–10 keV band is $2.84^{+0.80}_{-1.23} \times 10^{-13}$ erg cm^2 s^{-1} while the extrapolated flux to the 15–55 keV band is 5.8×10^{-13} erg cm^2 s^{-1}. The spectrum of A19 is compatible with an unabsorbed power-law model with a photon index of $2.02^{+0.56}_{-0.49}$. Its 2–10 keV flux is $7.76^{+0.45}_{-6.72} \times 10^{-14}$ erg cm^{-2} s^{-1} while extrapolated flux to the 15–55 keV band is 6.2×10^{-14} erg cm^2 s^{-1}. It is clear that A19 might contribute a non-negligible fraction (e.g., ∼25%) of the total flux detected in the BAT band while that is not the case for A20. Thus, when analyzing the cluster emission (below) we will also include, in all spectral fits, an absorbed power-law component representing the spectrum A19. The parameters of this absorbed power law will be allowed to vary within their 90% CL reported above.

A single-temperature plasma model (reported in Figure 16) with a temperature of $9.47^{+0.43}_{-0.44}$ and an abundance of 0.32 ± 0.06 solar successfully fits the *XMM-Newton* and *Swift*/BAT data. Our results are in good agreement with those derived in the 0.5–40 keV band by *BeppoSAX* (Ettori et al. 2001). This fit is good (χ^2/dof = 409.9/375), but it leaves some residuals at high energy. We then tried adding a second thermal model and obtained a better fit (e.g., χ^2/dof = 394.5/372). The improvement in the χ^2 is significant and the *F*-test yields a probability of $\sim 10^{-3}$ that it was produced by chance. The "cold" and "warm" components have a temperature of $3.76^{+2.80}_{-1.61}$ keV and $13.08^{+4.15}_{-2.69}$ keV, respectively, while their abundances are $0.46^{+0.49}_{-0.24}$ and $0.37^{+0.23}_{-0.14}$. Our results are in agreement with those obtained by Allen et al. (2001) using *Chandra*. Indeed, they showed that the temperature of the plasma within 100 kpc of the core is $\leqslant 5$ keV while its temperature stays approximately constant at $11.5^{+1.5}_{-1.6}$ keV beyond 200 kpc. Adding a power-law model to the baseline thermal model improves the fit only marginally ($\Delta\chi^2 = 6.1$ for two additional parameters), thus we consider the double-temperature thermal model as the best representation of our data set. This fit, together with the single-temperature thermal model, is shown in Figure 16.

The 99% CL upper limit on the 50–100 keV non-thermal flux, estimated using a power law with a photon index of 2.0, is 3.14×10^{-13} erg cm^{-2} s^{-1}. In order to compute the lower limit on the intensity of the magnetic field (see Table 4), we adopt for this cluster a value of the spectral index of $\alpha = 2$.

4. CLUSTERS MAGNETIC FIELD

The diffuse synchrotron radio emission (radio halos, relics, and mini-halos) proves the existence of magnetic fields and relativistic electrons in the ICM. If the non-thermal X-ray

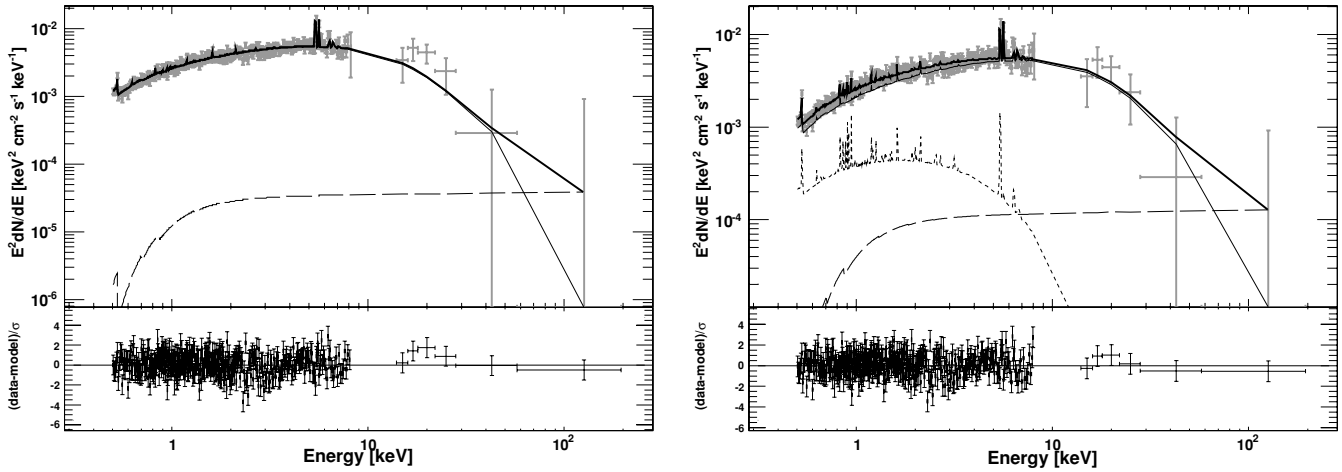

Figure 16. Left panel: spectrum of A2390 fitted with a single thermal model plus an absorbed power law (dashed line) to account for the emission of the AGN A19 (see the text for details). Right panel: spectrum of A2390 fitted with the sum of two thermal models (thin solid and short-dashed line) and an absorbed power law (dashed line) to account for the emission of AGN A19 (see the text for details).

emission results from IC scattering of the same population by the CMB, then the lack of a detection of a non-thermal component can be used to place a lower limit on the magnetic fields B in clusters. Indeed, the ratio of radio to IC flux scales proportionally to $B^{\alpha+1}$. Following Harris & Romanishin (1974), we estimate the lower limit on B (the volume averaged component along the line of sight) as explained in Ajello et al. (2009a), but taking into account the redshift correction. We model the IC emission as a power law with index 2 (see e.g., Reimer et al. 2004, for more details). The value of the diffuse radio flux is difficult to measure due to the presence of individual radio sources and to the variability of the spectral index with the distance from the center. Therefore, the magnetic field intensities listed in Table 4 have to be taken as order-of-magnitude estimates. We find magnetic fields that are typically a fraction of a μG, thus far from equipartition. Note that A2390 is the only cluster for which we evaluate the magnetic field related to the radio mini-halo—and hence to the central AGN—rather than to a more extended radio halo or radio relic. It was not possible to estimate the lower limit on the magnetic field intensity for a few of the clusters reported in Table 4 for which there are no detections of radio halos reported in the literature at this time. Given the fact that the sensitivity of BAT in its band is of the order of $\sim 5 \times 10^{-12}$ erg cm^{-2} s^{-1} and thus comparable to the sensitivities reached (in other bands) by other observatories (e.g., HEAO-1, *RXTE*, *BeppoSAX*, etc.), the upper limits reported in Table 4 are similar to those obtained by other authors (e.g., see Rephaeli et al. 1987; Henriksen 1998; Rephaeli et al. 1999; Rossetti & Molendi 2004, and references therein).

5. CONCLUSIONS

The present work combines *Swift*/BAT and *XMM-Newton* observations to investigate the presence of a hard X-ray excess in the spectra of 10 galaxy clusters detected in the ongoing BAT survey (Cusumano et al. 2010). Our results agree with our previous findings for a sample of 10 clusters (Ajello et al. 2009a)—i.e., most of the clusters' spectra are best described by a multi-temperature thermal model. The only exception is represented by the Bullet cluster and A3667, for which we find evidence (at the 4.4σ and 4.6σ level, respectively) for a hard X-ray excess.

For the Bullet cluster, our data point to the existence of a power-law-like component with a photon index of $1.86^{+1.25}_{-0.14}$ and a 20–100 keV flux of $3.4^{+1.1}_{-1.0} \times 10^{-12}$ erg cm^{-2} s^{-1}. The flux of this component is found to be in good agreement with similar values reported by Petrosian et al. (2006) and Million & Allen (2009). Using the flux reported above and radio data available in the literature, we estimate that the volume-averaged magnetic field should have an intensity of $\sim$0.2 μG.

The case of A3667 is different. Indeed for A3667, the excess can be explained in terms of a hot component with a temperature of $13.5^{+6.9}_{-2.2}$ keV. Our findings are in agreement with the results from *Suzaku* (Nakazawa et al. 2009). The lack of a central radio halo in A3667, supports the thermal origin of the hard X-ray excess.

The Norma cluster is a special cluster for a different reason. It is the second cluster, along with Coma (Ajello et al. 2009a), to be resolved spatially by BAT. The BAT spectrum shows (albeit with low statistics) that the temperature is around $\sim$10 keV and thus hotter than the temperature ($\sim$5 keV) determined at lower energies with *XMM-Newton*. Since it is resolved by BAT, special care must be taken when analyzing data from this cluster and a detailed analysis will be presented elsewhere.

Three of the detected clusters (PKS 0745-19, A1795, and A2390) have a bright cool core, while three (Bullet cluster, A2256, and A3627) are undergoing a major merger. A1914, A85, and A3667 show signs of a minor merger as well. Six clusters (A401, Bullet cluster, PKS 0745-19, A1914, A2256, and A3667) have a radio halo or a radio relic. The best spectral fits are given by the sum of two thermal components for five clusters (A85, A401, PKS 0745-19, A3667, and A2390). The other four clusters (A1795, A1914, A2256, and A2390) are successfully fit with a relatively hot single-temperature profile.

The upper limit to the non-thermal emission (in the 50–100 keV band) is around 10^{-12} erg cm^{-12} s^{-1} for most clusters. Once again, our results indicate that the hard X-ray emission from galaxy clusters is mostly thermal and probably related to post-shock regions (in the case of merging clusters) or hot regions outside the cool core (in the case of relaxed clusters). It is reasonable to assume that the relativistic electrons observed in the radio band, produce a power-law-like emission at higher energies due to IC scattering off CMB photons (e.g., Rephaeli 1979; Sarazin 1999). In this case, we used the presented

results to obtain lower limits on the clusters' magnetic fields. In this way, we find magnetic fields of the order of a fraction of μGauss that are far from equipartition and in agreement with previous similar estimates. These limits are generally a factor of 10 below the estimates obtained using Faraday rotation measures (e.g., Clarke et al. 2001; Guidetti et al. 2008; Bonafede et al. 2010).

The Bullet cluster is the only one that stands out among the clusters detected so far by BAT for the evidence of a power-law-like, hard X-ray excess. However, many factors make this cluster special and unique, among them: the intermediate redshift and the violent merging activity. The merging process powers shocks (e.g., Markevitch et al. 2002) where CRs can be accelerated efficiently. The energy density of the CMB, whose photons constitute the targets for the electrons, scales with $(1 + z)^4$, and thus is a factor of $\sim$2.8 larger than at redshift zero. Both things probably concur in producing the "bright" non-thermal component observed in this cluster.

A critical review from the referee dramatically improved this paper. P.R. is supported by the Pappalardo Postdoctoral Fellowship in Physics at MIT. N.C. was partially supported from NASA grant NNX07AV03G. M.A. and P.R. wish to acknowledge Balú Rebusco for his positivity. This research has made use of the NASA/IPAC Extragalactic Database (NED) which is operated by the Jet Propulsion Laboratory, of data obtained from the High Energy Astrophysics Science Archive Research Center (HEASARC) provided by NASA's Goddard Space Flight Center, and of the SIMBAD Astronomical Database which is operated by the Centre de Données Astronomiques de Strasbourg.

Facilities: Swift (BAT/XRT), *XMM*

REFERENCES

Ajello, M., Greiner, J., Kanbach, G., Rau, A., Strong, A. W., & Kennea, J. A. 2008a, ApJ, 678, 102
Ajello, M., et al. 2008b, ApJ, 689, 666
Ajello, M., et al. 2008c, ApJ, 673, 96
Ajello, M., et al. 2009a, ApJ, 690, 367
Ajello, M., et al. 2009b, ApJ, 699, 603
Alikberov, K. D., Dagkesamanskii, R. D., & Shutenkov, V. R. 1983, SvA, 27, 6
Allen, S. W., Ettori, S., & Fabian, A. C. 2001, MNRAS, 324, 877
Allen, S. W., Fabian, A. C., & Kneib, J. P. 1996, MNRAS, 279, 615
Anders, E., & Grevesse, N. 1989, Geochim. Cosmochim. Acta, 53, 197
Ando, S., & Nagai, D. 2008, MNRAS, 385, 2243
Arnaud, K. A. 1996, in ASP Conf. Ser. 101, Astronomical Data Analysis Software and Systems V, ed. G. H. Jacoby & J. Barnes (San Francisco, CA: ASP), 17
Arnaud, K. A., Johnstone, R. M., Fabian, A. C., Crawford, C. S., Nulsen, P. E. J., Shafer, R. A., & Mushotzky, R. F. 1987, MNRAS, 227, 241
Arnaud, M., Lachieze-Rey, M., Rothenflug, R., Yamashita, K., & Hatsukade, I. 1991, A&A, 243, 56
Arnaud, M., Neumann, D. M., Aghanim, N., Gastaud, R., Majerowicz, S., & Hughes, J. P. 2001, A&A, 365, L80
Avni, Y. 1976, ApJ, 210, 642
Bacchi, M., Feretti, L., Giovannini, G., & Govoni, F. 2003, A&A, 400, 465
Baldi, A., Ettori, S., Mazzotta, P., Tozzi, P., & Borgani, S. 2007, ApJ, 666, 835
Ball, R., Burns, J. O., & Loken, C. 1993, AJ, 105, 53
Barthelmy, S. D., et al. 2005, Space Sci. Rev., 120, 143
Baum, S. A., & O'Dea, C. P. 1991, MNRAS, 250, 737
Boehringer, H., Neumann, D. M., Schindler, S., & Kraan-Korteweg, R. C. 1996, ApJ, 467, 168
Boehringer, H., Tanaka, Y., Mushotzky, R. F., Ikebe, Y., & Hattori, M. 1998, A&A, 334, 789
Böhringer, H., et al. 2000, ApJS, 129, 435
Bonafede, A., Feretti, L., Murgia, M., Govoni, F., Giovannini, G., Dallacasa, D., Dolag, K., & Taylor, G. B. 2010, arXiv:1002.0594
Bradač, M., et al. 2006, ApJ, 652, 937
Bridle, A. H., & Fomalont, E. B. 1976, A&A, 52, 107
Briel, U. G., Finoguenov, A., & Henry, J. P. 2004, A&A, 426, 1
Briel, U. G., & Henry, J. P. 1996, ApJ, 472, 131
Briel, U. G., et al. 1991, A&A, 246, L10
Buote, D. A., & Tsai, J. C. 1996, ApJ, 458, 27
Burlon, D., Ajello, M., & Greiner, J. 2010, ApJ, submitted
Burns, J. O. 1990, AJ, 99, 14
Carter, J. A., & Read, A. M. 2007, A&A, 464, 1155
Chen, Y., Ikebe, Y., & Böhringer, H. 2003, A&A, 407, 41
Churazov, E., Forman, W., Vikhlinin, A., Tremaine, S., Gerhard, O., & Jones, C. 2008, MNRAS, 388, 1062
Clarke, T. E., & Ensslin, T. 2006, Astron. Nachr., 327, 553
Clarke, T. E., Kronberg, P. P., & Böhringer, H. 2001, ApJ, 547, L111
Clowe, D., Bradač, M., Gonzalez, A. H., Markevitch, M., Randall, S. W., Jones, C., & Zaritsky, D. 2006, ApJ, 648, L109
Clowe, D., Gonzalez, A., & Markevitch, M. 2004, ApJ, 604, 596
Crawford, C. S., Gandhi, P., Fabian, A. C., Wilman, R. J., Johnstone, R. M., Barger, A. J., & Cowie, L. L. 2002, MNRAS, 333, 809
Cusumano, G., et al. 2010, A&A, 510, A48
Dagkesamanskii, R. D., Kuzmin, A. D., Gubanov, A. G., & Slee, O. B. 1982, MNRAS, 200, 971
De Grandi, S., & Molendi, S. 1999, A&A, 351, L45
De Grandi, S., & Molendi, S. 2001, ApJ, 551, 153
De Grandi, S., & Molendi, S. 2002, ApJ, 567, 163
Dunn, R. J. H., & Fabian, A. C. 2006, MNRAS, 373, 959
Dunn, R. J. H., Fabian, A. C., & Taylor, G. B. 2005, MNRAS, 364, 1343
Durret, F., Lima Neto, G. B., & Forman, W. 2005, A&A, 432, 809
Ebeling, H., Voges, W., Bohringer, H., Edge, A. C., Huchra, J. P., & Briel, U. G. 1996, MNRAS, 281, 799
Edge, A. C., Stewart, G. C., & Fabian, A. C. 1992, MNRAS, 258, 177
Edge, A. C., Stewart, G. C., Fabian, A. C., & Arnaud, K. A. 1990, MNRAS, 245, 559
Ensslin, T. A., Biermann, P. L., Klein, U., & Kohle, S. 1998, A&A, 332, 395
Ettori, S., Allen, S. W., & Fabian, A. C. 2001, MNRAS, 322, 187
Ettori, S., Fabian, A. C., Allen, S. W., & Johnstone, R. M. 2002, MNRAS, 331, 635
Ettori, S., Fabian, A. C., & White, D. A. 1998, MNRAS, 300, 837
Fabian, A. C., Sanders, J. S., Ettori, S., Taylor, G. B., Allen, S. W., Crawford, C. S., Iwasawa, K., & Johnstone, R. M. 2001, MNRAS, 321, L33
Fabian, A. C., et al. 1985, MNRAS, 216, 923
Fenimore, E. E., & Cannon, T. M. 1978, Appl. Opt., 17, 337
Finoguenov, A., Böhringer, H., & Zhang, Y.-Y. 2005, A&A, 442, 827
Finoguenov, A., Briel, U. G., Henry, J. P., Gavazzi, G., Iglesias-Paramo, J., & Boselli, A. 2004, A&A, 419, 47
Fujita, Y., Koyama, K., Tsuru, T., & Matsumoto, H. 1996, PASJ, 48, 191
Fusco-Femiano, R., Dal Fiume, D., Orlandini, M., Brunetti, G., Feretti, L., & Giovannini, G. 2001, ApJ, 552, L97
Fusco-Femiano, R., Landi, R., & Orlandini, M. 2005, ApJ, 624, L69
Fusco-Femiano, R., Landi, R., & Orlandini, M. 2007, ApJ, 654, L9
Fusco-Femiano, R., et al. 2000, ApJ, 534, L7
Ge, J. P., & Owen, F. N. 1993, AJ, 105, 778
Gehrels, N., et al. 2004, ApJ, 611, 1005
George, M. R., Fabian, A. C., Sanders, J. S., Young, A. J., & Russell, H. R. 2009, MNRAS, 395, 657
Giovannini, G., & Feretti, L. 2000, New Astron., 5, 335
Giovannini, G., Feretti, L., Venturi, T., Kim, K.-T., & Kronberg, P. P. 1993, ApJ, 406, 399
Giovannini, G., Tordi, M., & Feretti, L. 1999, New Astron., 4, 141
Govoni, F., Markevitch, M., Vikhlinin, A., VanSpeybroeck, L., Feretti, L., & Giovannini, G. 2004, ApJ, 605, 695
Guidetti, D., Murgia, M., Govoni, F., Parma, P., Gregorini, L., de Ruiter, H. R., Cameron, R. A., & Fanti, R. 2008, A&A, 483, 699
Guthrie, B. N. G. 1974, MNRAS, 168, 15
Hanisch, R. J. 1982, A&A, 111, 97
Harris, D. E., & Miley, G. K. 1978, A&AS, 34, 117
Harris, D. E., & Romanishin, W. 1974, ApJ, 188, 209
Henriksen, M. 1998, PASJ, 50, 389
Henriksen, M. 1999, ApJ, 511, 666
Hill, J. M., Hintzen, P., Oegerle, W. R., Romanishin, W., Lesser, M. P., Eisenhamer, J. D., & Batuski, D. J. 1988, ApJ, 332, L23
Ikebe, Y., Reiprich, T. H., Böhringer, H., Tanaka, Y., & Kitayama, T. 2002, A&A, 383, 773
Inoue, S., Aharonian, F. A., & Sugiyama, N. 2005, ApJ, 628, L9
Johnson, M. W., Cruddace, R. G., Wood, K. S., Ulmer, M. P., & Kowalski, M. P. 1983, ApJ, 266, 425
Jones, C., & Forman, W. 1999, ApJ, 511, 65
Jones, P. A., & McAdam, W. B. 1996, MNRAS, 282, 137

Kaastra, J. S., et al. 2008, Space Sci. Rev., 134, 1
Karachentsev, I. D., & Kopylov, A. I. 1980, MNRAS, 192, 109
Kempner, J. C., & Sarazin, C. L. 2001, ApJ, 548, 639
Kirsch, M. G., et al. 2005, Proc. SPIE, 5898, 22
Knopp, G. P., Henry, J. P., & Briel, U. G. 1996, ApJ, 472, 125
Kowalski, M. P., Cruddace, R. G., Wood, K. S., & Ulmer, M. P. 1984, ApJS, 56, 403
Kraan-Korteweg, R. C., Woudt, P. A., Cayatte, V., Fairall, A. P., Balkowski, C., & Henning, P. A. 1996, Nature, 379, 519
Kulkarni, V. K., Mantovani, F., & Pauliny-Toth, I. I. K. 1990, A&AS, 82, 41
Liang, H., Hunstead, R. W., Birkinshaw, M., & Andreani, P. 2000a, ApJ, 544, 686
Liang, H., Hunstead, R. W., Birkinshaw, M., & Andreani, P. 2000b, ApJ, 544, 686
Lumb, D. H., Warwick, R. S., Page, M., & De Luca, A. 2002, A&A, 389, 93
Lutovinov, A. A., Vikhlinin, A., Churazov, E. M., Revnivtsev, M. G., & Sunyaev, R. A. 2008, ApJ, 687, 968
Markevitch, M., Forman, W. R., Sarazin, C. L., & Vikhlinin, A. 1998, ApJ, 503, 77
Markevitch, M., Gonzalez, A. H., Clowe, D., Vikhlinin, A., Forman, W., Jones, C., Murray, S., & Tucker, W. 2004, ApJ, 606, 819
Markevitch, M., Gonzalez, A. H., David, L., Vikhlinin, A., Murray, S., Forman, W., Jones, C., & Tucker, W. 2002, ApJ, 567, L27
Markevitch, M., Vikhlinin, A., & Mazzotta, P. 2001, ApJ, 562, L153
McHardy, I. 1978, MNRAS, 184, 783
McMillan, S. L. W., Kowalski, M. P., & Ulmer, M. P. 1989, ApJS, 70, 723
Million, E. T., & Allen, S. W. 2009, MNRAS, 399, 1307
Miralda-Escude, J., & Babul, A. 1995, ApJ, 449, 18
Mitchell, R. J., Dickens, R. J., Burnell, S. J. B., & Culhane, J. L. 1979, MNRAS, 189, 329
Molendi, S., De Grandi, S., & Fusco-Femiano, R. 2000, ApJ, 534, L43
Molendi, S., & Gastaldello, F. 2009, A&A, 493, 13
Mushotzky, R. F., & Loewenstein, M. 1997, ApJ, 481, L63
Nagai, D., Vikhlinin, A., & Kravtsov, A. V. 2007, ApJ, 655, 98
Nakazawa, K., et al. 2009, PASJ, 61, 339
Nevalainen, J., Markevitch, M., & Lumb, D. 2005, ApJ, 629, 172
Nevalainen, J., Oosterbroek, T., Bonamente, M., & Colafrancesco, S. 2004, ApJ, 608, 166
Owen, F. N. 1975, ApJ, 195, 593
Owen, F. N., & Ledlow, M. J. 1997, ApJS, 108, 41
Owen, F. N., White, R. A., & Ge, J. 1993, ApJS, 87, 135
Peres, C. B., Fabian, A. C., Edge, A. C., Allen, S. W., Johnstone, R. M., & White, D. A. 1998, MNRAS, 298, 416
Petrosian, V., Madejski, G., & Luli, K. 2006, ApJ, 652, 948
Piccinotti, G., Mushotzky, R. F., Boldt, E. A., Holt, S. S., Marshall, F. E., Serlemitsos, P. J., & Shafer, R. A. 1982, ApJ, 253, 485
Pierre, M., Le Borgne, J. F., Soucail, G., & Kneib, J. P. 1996, A&A, 311, 413
Pierre, M., & Starck, J. 1998, A&A, 330, 801
Prestwich, A. H., Guimond, S. J., Luginbuhl, C. B., & Joy, M. 1995, ApJ, 438, L71
Read, A. M., & Ponman, T. J. 2003, A&A, 409, 395
Reimer, O., Pohl, M., Sreekumar, P., & Mattox, J. R. 2003, ApJ, 588, 155
Reimer, A., Reimer, O., Schlickeiser, R., & Iyudin, A. 2004, A&A, 424, 773
Renaud, M., Bélanger, G., Paul, J., Lebrun, F., & Terrier, R. 2006, A&A, 453, L5
Rengelink, R. B., Tang, Y., de Bruyn, A. G., Miley, G. K., Bremer, M. N., Roettgering, H. J. A., & Bremer, M. A. R. 1997, A&AS, 124, 259
Rephaeli, Y. 1979, ApJ, 227, 364
Rephaeli, Y., & Gruber, D. 2002, ApJ, 579, 587
Rephaeli, Y., & Gruber, D. 2003, ApJ, 595, 137
Rephaeli, Y., Gruber, D., & Blanco, P. 1999, ApJ, 511, L21
Rephaeli, Y., Gruber, D. E., & Rothschild, R. E. 1987, ApJ, 320, 139
Revnivtsev, M., Sazonov, S., Jahoda, K., & Gilfanov, M. 2004, A&A, 418, 927
Rhee, G. F. R. N., & Latour, H. J. 1991, A&A, 243, 38
Rizza, E., Burns, J. O., Ledlow, M. J., Owen, F. N., Voges, W., & Bliton, M. 1998, MNRAS, 301, 328
Rossetti, M., & Molendi, S. 2004, A&A, 414, L41
Rottgering, H. J. A., Wieringa, M. H., Hunstead, R. W., & Ekers, R. D. 1997, MNRAS, 290, 577
Ryu, D., & Kang, H. 2003, J. Korean Astron. Soc., 36, 105
Sakelliou, I., & Ponman, T. J. 2004, MNRAS, 351, 1439
Sanders, J. S., Fabian, A. C., & Allen, S. W. 2000, MNRAS, 318, 733
Sanders, J. S., Fabian, A. C., & Dunn, R. J. H. 2005, MNRAS, 360, 133
Sarazin, C. L. 1988, X-ray Emission from Clusters of Galaxies (Cambridge Astrophys. Series; Cambridge: Cambridge Univ. Press)
Sarazin, C. L. 1999, ApJ, 520, 529
Sarazin, C. L., & Kempner, J. C. 2000, ApJ, 533, 73
Segreto, A., Cusumano, G., Ferrigno, C., La Parola, V., Mangano, V., Mineo, T., & Romano, P. 2010, A&A, 510, A47
Skinner, G. K., Ponman, T. J., Hammersley, A. P., & Eyles, C. J. 1987, Ap&SS, 136, 337
Slee, O. B., Roy, A. L., Murgia, M., Andernach, H., & Ehle, M. 2001, AJ, 122, 1172
Sun, M., Donahue, M., Roediger, E., Nulsen, P. E. J., Voit, G. M., Sarazin, C., Forman, W., & Jones, C. 2010, ApJ, 708, 946
Tamura, T., Fukazawa, Y., Kaneda, H., Makishima, K., Tashiro, M., Tanaka, Y., & Bohringer, H. 1998, PASJ, 50, 195
Tamura, T., et al. 2001, A&A, 365, L87
Thierbach, M., Klein, U., & Wielebinski, R. 2003, A&A, 397, 53
Timokhin, A. N., Aharonian, F. A., & Neronov, A. Y. 2004, A&A, 417, 391
Tucker, W. H., Tananbaum, H., & Remillard, R. A. 1995, ApJ, 444, 532
Tucker, W., et al. 1998, ApJ, 496, L5
Tueller, J., et al. 2010, ApJS, 186, 378
Ulmer, M. P., Kowalski, M. P., & Cruddace, R. G. 1986, ApJ, 303, 162
Vikhlinin, A., Markevitch, M., & Murray, S. S. 2001, ApJ, 549, L47
Vikhlinin, A., Markevitch, M., Murray, S. S., Jones, C., Forman, W., & Van Speybroeck, L. 2005, ApJ, 628, 655
Watanabe, M., Yamashita, K., Furuzawa, A., Kunieda, H., & Tawara, Y. 2001, PASJ, 53, 605
Watson, M. G., et al. 2009, A&A, 493, 339
White, D. A. 2000, MNRAS, 312, 663
White, D. A., Jones, C., & Forman, W. 1997, MNRAS, 292, 419
Willson, M. A. G. 1970, MNRAS, 151, 1
Wood, K. S., et al. 1984, ApJS, 56, 507
Zhang, Y., Böhringer, H., Finoguenov, A., Ikebe, Y., Matsushita, K., Schuecker, P., Guzzo, L., & Collins, C. A. 2006, A&A, 456, 55
Zhang, Y.-Y., Finoguenov, A., Böhringer, H., Ikebe, Y., Matsushita, K., & Schuecker, P. 2004, A&A, 413, 49